CXCR7 promotes foetal myoblast fusion at muscle fiber tips independently of Myomaker via a ß1integrin-EGFR-dependent mechanism

Sonya Nassari (1, 2), Cédrine Blavet (1), Delphine Duprez (1)* and Claire Fournier-Thibault (1)*

(1)Sorbonne Université, Institut Biologie Paris Seine, CNRS UMR7622, Developmental Biology Laboratory, Inserm U1156, F-75005 Paris, France.

(2) New affiliation: Faculté de Médecine et des Sciences de la Santé, Department of Immunology and Cell Biology, Université de Sherbrooke, 3201 Rue Jean Mignault, Sherbrooke, Québec J1E 4K8, Canada.

*co-corresponding authors : claire.thibault@sorbonne-universite.fr

delphine.duprez@sorbonne-universite.fr

Abstract

Muscle growth must be tightly regulated during development in order to obtain the final muscle shape. Myoblast fusion is a critical step of muscle growth, driving the formation of syncytial myofibers attaching at both ends to tendons. We investigated the role of the CXCR7 chemokine receptor in foetal muscle growth during chicken limb development. We show that CXCR7 displays a regionalized expression at the tips of myofibers close to tendons in foetal limb muscles, which is exclusive to the central location of the fusion gene MYOMAKER (*TMEM8C* in chicken) in foetal muscles. CXCR7 promotes myoblast fusion independently of *TMEM8C* in chicken limb muscles and in foetal myoblast cultures and requires EGF receptor signalling. The CXCR7 ligand, CXCL12, expressed in connective tissue, increases ß1integrin activation at the myotendinous junction and CXCR7 expression at muscle tips, resulting in a fusion promoting effect independent from a direct binding of CXCL12 to CXCR7 receptor. Our results evidence a CXCR7-dependent/TMEM8C-independent fusion mechanism at the myofiber tips that regulates muscle growth at the tendon/muscle interface during foetal myogenesis.

Introduction

During development, skeletal muscle growth must be tightly regulated in order to obtain the final shape of each individual muscle. This process relies on muscle progenitors expressing the PAX3 and PAX7 transcription factors (Relaix et al., 2005; Hutcheson et al., 2009), which enter the myogenic program under the control of the Myogenic Regulatory Factors (MRFs), including the bHLH transcription factors MYF5, MYOD, MYOG and MRF4 (Buckingham and Rigby, 2014). The MRFs trigger the successive steps of muscle specification, differentiation and finally fusion, the ultimate phase of myogenesis, leading to the conversion of mononucleated muscle cells to multinucleated myofibers, the functional unit of skeletal muscle (Comai and Tajbakhsh, 2014; Esteves de Lima and Relaix, 2021). Distinct successives phases of myogenesis are observed during muscle development. Embryonic myogenesis involves fusion events between myoblasts, forming the nascent primary myofibers that define the scaffold of the future muscles (Besse et al., 2020; Kardon, 1998) and is followed by foetal myogenesis which involves myoblast fusion to embryonic myofibers and correspond to muscle growth (Biressi et al., 2007). Finally, muscle satellite cells establish between myofibers and basal lamina and are responsible for postnatal growth and repair of adult muscle (Stockdale, 1992). MYOG-positive cells are recognized to be the fusion competent cells and MYOG function is required for myoblast fusion (Ganassi et al., 2018; Hasty et al., 1993).

Myoblast fusion has been shown to depend on the transmembrane protein MYOMAKER during developmental, postnatal and regenerative myogenesis (Petrany and Millay, 2019). During development, MYOMAKER is required and sufficient for myoblast fusion in mice, chicken and zebrafish (Landemaine et al., 2014; Luo et al., 2015; Millay et al., 2013) and in chicken limbs, *TMEM8C* (MYOMAKER in chicken) is enriched in central versus tip regions of foetal muscles, similarly to the preferential central location of MYOG-positive fusion-competent cells (Esteves de Lima et al., 2022), suggesting a regionalization of fusion events in foetal muscles. Apart from the pivotal role of MYOMAKER, extrinsic factors have also been shown to regulate muscle fusion but these have been mostly identified during regenerative myogenesis (Horsley et al., 2003; Sotiropoulos et al., 2006) and are less characterized during developmental myogenesis. TGFß signaling has been identified as a negative regulator of myoblast fusion during muscle regeneration in mice (Girardi et al., 2021) and also during development in chicken embryos (Melendez et al., 2021). Inhibition of ERK pathway has been shown to drive fusion of myoblast to myotubes in myoblast cultures

and during muscle regeneration (Eigler et al., 2021).

Chemotactic factors, secreted by the muscle environment or the muscle itself are recognized as important regulators of myoblast migration, the prerequisite step required for a correct fusion process during myogenesis as well as adult muscle repair (Abmayr and Pavlath, 2012). During embryonic development, the CXCL12 chemokine has been shown to be expressed in the limb mesenchyme and inactivation of CXCR4 receptor, expressed in muscle progenitors, inhibits their migration from the somite to the limb (Vasyutina et al., 2005). Inactivation of CXCL12 has also been shown to decrease myoblast fusion without affecting myogenic differentiation both in C2C12 myoblasts (Ge et al., 2013) and in mouse primary myoblasts (Griffin et al., 2010) via CXCL12 binding to CXCR4 (Bae et al., 2008; Griffin et al., 2010). CXCL12 chemokine can also signal through CXCR7 receptor. Depending on the cell type or process, CXCR7 has been alternatively described as a scavenger receptor for CXCL12 ligand or a signalling receptor acting with or without CXCR4 (Koch and Engele, 2020). The involvement of CXCR7 during myogenesis is not well documented, as homozygous CXCR7 null mutation in mice led to birth lethality, due to ventricular septal defects and semilunar heart valve malformation (Gerrits et al., 2008; Sierro et al., 2007). Nevertheless, sparse *in vitro* studies highlight a CXCR7 function in the differentiation steps of C2C12 muscle cells (Hunger et al., 2012; Melchionna et al., 2010). Interestingly, a recent siRNA screen conducted on the C2C12 cell line to determine genes implicated in myoblast fusion identified CXCR7 among the genes necessary for this process (Melendez et al., 2021).

In this study, we investigated the function of CXCR7 receptor during chicken limb foetal myogenesis. We show that CXCR7 exhibits a regionalized expression at the tips of muscles at the transcript and protein levels, which is exclusive from the central location of *TMEM8C* transcripts in chicken limb foetal muscles. CXCR7 promotes myoblast fusion independently of TMEM8C in foetal muscles and involves EGF receptor signaling in myoblast cultures. The CXCR7 ligand, CXCL12, expressed in connective tissue (CT), increases ß1integrin activation and CXCR7 expression at muscle tips and mimics the fusion promoting effect of CXCR7. Our results evidence a CXCR7-dependent fusion mechanism at the myofiber tips in chicken limb foetal muscles that would regulate muscle growth and elongation at the tendon/muscle interface independently of TMEM8C.

Results

CXCR7 receptor is expressed in foetal myogenic cells

We and others have previously shown that *CXCL12* is expressed in CT during limb development (García-Andrés and Torres, 2010; Nassari et al., 2017; Vasyutina et al., 2005). Here, we investigated the expression pattern of the two CXCL12 receptors, CXCR4 and CXCR7, during limb foetal myogenesis by in situ hybridization and immunostaining. PAX7 and MF20 antibodies were used to visualize progenitor and differentiated muscle cells. At E5, CXCR4 was expressed near the mesenchymal region expressing *CXCL12* (Fig. 1a, b), in cells of the nascent limb vasculature and at a lower level in the dorsal and ventral muscle masses (Fig. 1b, (Vasyutina et al., 2005)). At this stage, *CXCR7* transcripts are expressed in developing cartilage and in some muscle progenitors (Fig. 1c). Detection of both receptors revealed that some cells co-expressed CXCR4 and *CXCR7* (Fig. 1d) and revelation of PAX7 antibody showed that CXCR7 was indeed expressed in some PAX7-positive progenitors (Fig. 1e-g). From E6, revelation of MEP21 antibody, which stained endothelial cells, underlined the expression of CXCR4 in limb vessels (Supp. Fig. 1a-c), while it was down-regulated in muscle cells (Supp. Fig. 1b, d). From E8, *CXCR7* transcripts (Fig. 1h, j, k) and protein (Fig. 1l) appeared mostly expressed to the tips of differentiated MF20-positive myotubes (Fig. 1m, n). At this stage, *CXCL12* expression in CT was faintly expressed near *CXCR7* expression at muscle tips (Fig. 1h, i) but surprisingly, a strict correlation between ligand and receptor expression was not observed. At E10, *CXCR7* expression at the tips of myotubes (Fig. 1o, q) was observed facing the MTJ revealed by the tendon marker *SCLERAXIS (SCX)*, (Fig. 1r, s), while *CXCL12* expression was detected in CT mostly around limb vessels (Fig. 1p, t), corresponding to the vascular CXCR4 expression (Supp. Fig. 1e, f; Nassari et al., 2017). These results show that during foetal myogenesis, CXCR7 is first expressed in a sub-population of PAX7-positive progenitors, then at the tips of differentiated myotubes while CXCR4 is downregulated in muscle cells and expressed in limb vessels around which *CXCL12* expression is mostly located.

CXCR7 receptor promotes foetal myoblast fusion during chicken limb development

In order to elucidate the role of CXCR7 in foetal myogenesis, functional assays were performed by overexpressing the wild-type form of the *CXCR7* receptor or a dominant-negative form of the *CXCR7* receptor (*dnCXCR7*) in forelimbs of chicken embryos using the avian RCAS retrovirus system. The *dnCXCR7* construct lacked the carboxy-terminus part of

the receptor, impairing *CXCR7* internalization and signalling, without affecting its binding to CXCL12 ligand (Ray et al., 2013). Pellets of RCAS-*CXCR7* or RCAS-*dnCXCR7* producing chicken fibroblasts were grafted into E4 limbs to allow virus spread into dividing cells and induce gene overexpression (Fig. 2A; (Havis et al., 2016)). Embryos were collected 6 days later and muscles from grafted and control limbs were analyzed by performing 3D-reconstruction of MF20 whole-mount immunostaining. Overexpression of RCAS-*dnCXCR7* and RCAS-*CXCR7* both resulted in changes in muscle morphogenesis when compared to controls (Fig. 2Ba-d, Ca-d). Volume and length analyses in 3D-reconstructed muscles showed that most muscles expressing *dnCXCR7* exhibited a reduced volume and length while muscles overexpressing *CXCR7* have mostly an increased volume and length (Fig. 2Be, f, Ce, f).

To understand these phenotypes, infected and control wings were transversally sectioned and immunostained with PAX7, MYOG and MF20 antibodies. Analysis of sections showed that muscles overexpressing the *dn-CXCR7* form appeared smaller (Fig. 3c) when compared to controls (Fig. 3a), a phenotype confirmed by area measurements of the cross-sections of each muscle in the infected region (Fig. 3d). Comparison of transverse sections taken at the same longitudinal level in individual muscles (Fig. 3e) showed that *dn-CXCR7* expressing muscles were not only smaller when compared to controls but also shorter, as illustrated by the strong reduction of muscle surface at the tips compared to the bulk (50% versus 30% in the EMU muscle, Fig. 3f). Quantification of muscle cell proliferation, number of PAX7- and MYOG-positive cells on sections revealed no differences between *dnCXCR7*-expressing and control muscles (Supp. Fig. 2A, Fig. 3g), showing that muscle differentiation was not affected by *CXCR7* loss-of-function. However, *dnCXCR7* overexpression induced a significant decrease in the percentage of MYOG-positive myonuclei into myotubes when compared to control (Fig. 3h, i), showing that myoblast fusion was affected. This effect was confirmed by the quantification of the myofiber nuclei versus the total number of nuclei, which showed that the myoblast fusion index was decreased in *dnCXCR7* expressing muscles when compared to controls (Fig. 3j, k). These data showed that inhibition of CXCR7 receptor in foetal muscles decreases myoblast fusion during chicken limb development.

Conversely, most muscles overexpressing *CXCR7* appeared larger (Fig. 4b, c) when compared to control muscles (Fig. 4a), as assessed by the larger muscle areas observed in *CXCR7* expressing muscles when compared to controls (Fig. 4d). Comparison of transverse sections taken at the same longitudinal level (Fig. 4e) showed that the increase in muscle surface in *CXCR7* expressing EDC muscle was stronger at the tips compared to the bulk (150% versus 120%, Fig. 4f), suggesting that infected muscles were not only bigger but also

longer. Quantification of muscle cell proliferation, number of PAX7-positive and MYOG-positive cells on sections revealed no differences between *CXCR7*-expressing and control muscles (Supp. Fig. 2B, Fig. 4g), showing that muscle differentiation was not affected by *CXCR7* gain-of-function. *CXCR7* overexpression induced a significant increase in the percentage of MYOG-positive myonuclei into myotubes when compared to control (Fig. 3h, i), showing that myoblast fusion was increased. This effect was confirmed by the quantification of myoblast fusion index, which was increased in *CXCR7* expressing muscles when compared to controls (Fig. 4j, k). Taken together, these results show that CXCR7 receptor is required for the correct myoblast fusion process in limbs during chicken foetal development.

CXCR7 receptor promotes myoblast fusion in myoblast cultures

To understand CXCR7 function on myoblast fusion, we turned to *in vitro* experiments using primary cell cultures of foetal myoblasts derived from forelimbs of E10 chicken embryos. After 5 days of culture, in situ hybridization and immunostaining for CXCR7, PAX7 and MF20 revealed that *CXCR7* mRNA and protein were observed in some but not all PAX7 progenitors (Supp. Fig. 3Aa-c), as observed *in vivo*. In myotubes, CXCR7 was strongly expressed around most myonuclei but not all and did not display a restricted expression at the tips, as observed in chicken limb muscles (Supp. Fig. 3Ad-f; Fig. 1).

Foetal myoblasts were transfected with RCAS-*dnCXCR7*, RCAS-*CXCR7* or empty RCAS as a control and grown *in vitro* for 2 days in proliferation medium and 3 days in differentiation conditions. Analysis of the number of EDU-positive cells after 2 days of culture demonstrated that proliferation was not modified in primary cultures or in the PAX7-positive progenitors in *dnCXCR7*-expressing cells compared to controls (Supp. Fig. 3Ba). Consistently, no change in the number of PAX7- (Supp. Fig. 3Bb) and MYOG-positive cells (Fig. 5Ad-f) was observed in these conditions, showing that muscle cell specification and differentiation were not affected. However, *dnCXCR7* overexpression in foetal myoblasts *in vitro* led to a decrease in the number of myotubes (Fig. 5Aa-c) and in the number of MYOG-positive nuclei into the myotubes when compared to controls (Fig. 5Ad, e, g), resulting in a decrease in the myoblast fusion index (Fig. 5Ah) and in the number of nuclei per myotube (Fig. 5Ai). Interestingly, *dnCXCR7* overexpression did not modify the expression of the specific muscle fusogene *TMEM8C* (Fig. 5Aj). These results show that *CXCR7* inactivation in chicken foetal myoblast cultures reduced myoblast fusion without affecting muscle differentiation and *TMEM8C* expression.

Conversely, *CXCR7* overexpression in chick foetal myoblasts *in vitro* resulted in an increase in the number of myotubes (Fig. 5Ba-c). Cell proliferation was not affected in the whole culture and in PAX7-positive progenitors (Supp. Fig. 3Ca). No change in the number of PAX7- (Supp. Fig. 3Cb) and MYOG- positive cells (Fig. 5Bd-f) was observed but *CXCR7* overexpression in foetal myoblasts induced a significant increase in the number of MYOG-positive nuclei into the myotubes (Fig. 5Bd, e, g), leading to an increase in myoblast fusion index (Fig. 5Bh) and in the number of nuclei per myotube (Fig. 5Bi). Conversely, *CXCR7* overexpression did not modify *TMEM8C* expression (Fig. 5Bj). These results show that overexpression of *CXCR7* in chicken limbs increased myoblast fusion *in vitro* without affecting differentiation and *TMEM8C* expression.

Because myoblast fusion could be affected by the ability of foetal myoblasts to migrate, we tested the migration capacity of myoblasts under *CXCR7* loss- or gain-of-function conditions. *DnCXCR7*- or *CXCR7*-transfected foetal myoblasts were cultured in proliferation conditions until confluence and cells were scratched from the plate to create a wound. The ability of cultured cells and PAX7-positive cells to refill the gap was monitored after 48h of culture and showed that neither *CXCR7* loss- or gain-of-function modified the ability of PAX7-positive muscle progenitors to migrate (Supp. Fig. 4), demonstrating that the CXCR7 effect on myoblast fusion did not result from changes in the migration capacity of muscle progenitors.

CXCR7 promotes myoblast fusion independently of the muscle specific TMEM8C fusogene

We observed that CXCR7 gain- and loss-of-function in myoblast cultures did not affect the expression of the muscle specific TMEM8C fusogene (Fig. 5). In order to define whether the CXCR7 fusion-promoting effect was linked to TMEM8C, we analyzed the expression patterns of *CXCR7* and *TMEM8C* during foetal myogenesis. Indeed, we have recently shown that during chicken foetal myogenesis, *TMEM8C* transcripts are preferentially located in central regions of chicken limb foetal muscles and excluded from muscle tips (Esteves de Lima et al., 2022) where *CXCR7* transcripts are expressed (Fig. 1). Detection of both transcripts on transverse sections of E5, E6 and E10 limbs showed that *TMEM8C* and *CXCR7* expression did not overlapped in muscle cells (Fig. 6Aa-i). We then analyzed the consequences of *CXCR7* gain- and loss-of-function on *TMEM8C* expression in chicken limb muscles and found that *TMEM8C* expression was not affected by deregulation of CXCR7 signalling (Fig. 6Ba-c), as observed in myoblast cultures (Fig. 5). To confirm that the CXCR7 fusion effect was acting independently of TMEM8C, we blocked the TMEM8C-dependent

fusion by transfecting a specific chick *siTMEM8C* in myoblast cultures (Luo et al., 2015) and tested the consequences of CXCR7 gain- and loss-of-function in these conditions. Cells transfected with *siTMEM8C* showed a 50% reduction in the fusion index when compared to controls (Fig. 6Ca, b), as previously described (Luo et al., 2015). Conversely, when myoblasts were transfected simultaneously with *siTMEM8C* and *CXCR7*, they displayed a fusion index nearly equivalent to control cultures, showing that the CXCR7 fusion effect can occur in the absence of TMEM8C (Fig. 6Ca, b). In addition, myoblast cultures simultaneously transfected with *siTMEM8C* and *dn-CXCR7* exhibited a 10% lower fusion index than the one observed in myoblasts only transfected with *siTMEM8C* (Fig. 6Ca, b), showing that the loss-of-function of CXCR7 can affect myoblast fusion even in the absence of TMEM8C. The non-overlapping expression pattern of *CXCR7* and *TMEM8C* in foetal muscles, the unchanged *TMEM8C* expression levels in *CXCR7* functional experiments and the observations that *CXCR7* had an effect on myoblast fusion even in the absence of functional *TMEM8C* led us to conclude that the fusion promoting effect of *CXCR7* is independent of *TMEM8C*.

EGF receptor is required for the CXCR7 fusion promoting effect in myoblast culture:

CXCR7 receptor can act to regulate proliferation and migration processes or as a ligand scavenger (Koch and Engele, 2020), but to date, it has not been described as a fusogen protein and our results show that its fusion effect is independent of TMEM8C. As it has been shown that CXCR7 can physically interact with EGFR (Singh and Lokeshwar, 2011) and that EGFR phosphorylation is increased during myogenesis (Horikawa et al., 1999) and required for myoblast differentiation (Santos-Zas et al., 2016), we investigated whether EGFR could be involved in the CXCR7 effect on myoblast fusion. We first analyzed the expression pattern of the phosphorylated form of EGFR (pEGFR) during chicken limb foetal myogenesis. At E6, pEGFR was not expressed in muscle cells (Fig. 7Aa), while from E8, nuclear pEGFR was observed in most muscle cells (Fig. 7Ab, c, d). At this stage, most myonuclei expressing CXCR7 at the tips of myotubes exhibited a nuclear expression of pEGFR (Fig. 7Ae). Analysis of pEGFR staining in myoblast cultures showed a cytoplasmic expression in PAX7-positive cells (Fig. 7Ba) while a nuclear expression was observed in myotubes (Fig. 7Bb). To test whether CXCR7 acts through EGFR signalling to promote myoblast fusion, we blocked the tyrosine kinase activity of EGFR in CXCR7 gain-of-function experiments in myoblast cultures. Foetal myoblasts were transfected with RCAS-*CXCR7* and treated with PD153035 reagent which inhibits the EGFR tyrosine kinase activity by acting as a selective ATP competitive inhibitor of phosphorylation (Fry et al., 1994). The decrease of pEGFR

expression in PD153035-treated cultures was a witness of the efficacy of the inhibitor. PD153035-treated cultures showed a decrease in foetal myoblast fusion (Fig. 7Cd-f, m) when compared to controls (Fig. 7Ca-c, m). As described above, *CXCR7* overexpression in cultured chicken foetal myoblasts led to a significant increase in the number of myotubes and in myoblast fusion index (Fig. 7Cg-i, m). However, this effect was not observed when *CXCR7* transfected cultures were treated with PD153035 (Fig. 7Cj-l). Indeed, such cultures exhibited a myoblast fusion index nearly similar to PD153035-treated cultures (Fig. 7Cm). These data show that EGFR is required for the fusion promoting effect of CXCR7 in chicken foetal myoblasts.

CXCL12 overexpression increases myoblast fusion in chicken limb muscles, while having no effect on myoblast cultures.

The CXCL12 ligand of CXCR7 receptor is expressed in CT surrounding muscles during limb development (Fig. 1;García-Andrés and Torres, 2010; Nassari et al., 2017; Vasyutina et al., 2005). Consequently, we tested whether CXCL12 coming from the CT could be involved in the effect of CXCR7 on foetal myoblast fusion of chicken limbs. A stable vector containing the chicken *CXCL12* sequence and the TOMATO gene as a reporter (Nassari et al., 2017) was electroporated in the forelimb lateral plate to overexpress *CXCL12* specifically in limb CT. Electroporation was performed at E2.5 and electroporated and contralateral limbs were analyzed at E9 (Fig. 8Aa, b) by immunostaining on sections with PAX7, MYOG and MF20 antibodies. CXCL12 overexpression was assessed by TOMATO fluorescence (Fig. 8Ab, Bb, e). Analysis of sections showed that muscles surrounded by *CXCL12* overexpression in the CT appeared larger (Fig. 8Bb, e) when compared to controls (Fig. 8Ba, e), as shown by area measurements of each muscle in the electroporated region, which were increased when compared to controls (Fig. 8Bc). Comparison of transverse sections taken at the same longitudinal level (Fig. 8Bd) showed that the increase in muscle surface in EDC muscle surrounded by CXCL12 expression was stronger at the tips compared to the bulk (150% versus 130%, Fig. 8f), suggesting that muscles in the electroporated region were not only larger but also longer, as observed for *CXCR7*-overexpressing limb muscles (Fig. 4). Quantification of muscle cell proliferation, number of PAX7- (Sup. Fig. 2C) and MYOG-positive cells (Fig. 8Bf) revealed no differences between muscles in control and electroporated forelimbs. *CXCL12* overexpression in CT induced a significant increase in the number of MYOG-positive nuclei inside the myotubes (Fig. 8Bg, h) and in the myoblast fusion index (Fig. 8Bi, j) when compared to controls. In addition, *CXCL12* overexpression in

CT did not modify the expression of the fusion gene *TMEM8C* (Fig. 8C). These results show that *CXCL12* overexpression in limb CT increased foetal myoblast fusion.

Because CXCL12 expressed in limb CT mimicked the fusion effect of CXCR7 in chicken limb muscles (Fig. 4), we tested whether this effect was observed in myoblast cultures. Primary cultures of chicken embryonic fibroblasts were transfected with RCAS-*CXCL12,* cultured for 2 days and the culture medium was collected to prepare CXCL12-concentrated supernatant, which was added to foetal myoblast culture medium. In some experiments, CXCL12 recombinant protein was added to foetal myoblasts grown in N2 minimum medium without serum to avoid a possible effect of CXCL12 contained in the culture serum. In both cases, primary muscle cells were cultured for 2 days in proliferation medium and 3 days in differentiation conditions (Sup. Fig. 5A). Surprisingly, MF20 immunostaining did not revealed differences in the number of myotubes in the presence of CXCL12, compared to controls (Sup. Fig. 5Ba-d). Cell proliferation (Sup. Fig. 5Be, f), number of PAX7-positive cells (Sup. Fig. 5Bg) and myoblast fusion (Sup. Fig. 5Bh, i) were not modified either by the addition of CXCL12 supernatant or CXCL12 recombinant protein. These results show that an exogenous source of CXCL12 does not regulate foetal myoblast fusion in cultures, suggesting that CXCL12 does not act directly via binding to CXCR7 receptor to activate myoblast fusion in chicken limb muscles.

Fusion effect of CXCR7 is promoted by a CXCL12-dependent activation of ß1 integrins

We have previously shown that CXCL12 induces the expression of CT markers and extracellular matrix genes in chicken embryonic limb, among which collagens (Nassari et al., 2017; Vallecillo-García et al., 2017). Collagens bind to integrin receptors that are required for the formation of MTJs (Martin-Bermudo, 2000; Mayer et al., 1997; Valdivia et al., 2017) and ß1integrins are recognized as regulators of myoblast fusion (Schwander et al., 2003). Moreover, ß1integrin activation consecutive to stromal extracellular matrix remodelling has been shown to increase CXCR7 expression in tumor cells (Kiss et al., 2013; Windus et al., 2014).

To analyze the effect of CXCL12 on ß1integrin activation, *CXCL12* was overexpressed in limb CT by electroporation of the forelimb lateral plate and sections of control and experimental limbs were immunostained with TASC, an antibody that specifically recognized the activated form of ß1integrin (Neugebauer and Rekhart, 1991). As expected, activated ß1integrins are expressed at the MTJ in control limbs (Fig. 9Ab, f). *CXCL12* overexpression in limb CT induced a significant enlargement of ß1integrin activation at the level of the MTJ

(Fig. 9Ad, g) where Tomato, reflecting ectopic CXCL12, was observed (Fig. 9Ac, h). ß1integrin activation was also enhanced around the cartilage elements in Tomato-positive regions in electroporated limbs compared to controls (Fig. 9Ad, g). In addition, an enlargement of CXCR7 expression was observed nearby the activated ß1integrin at the MTJ in muscles surrounded by CXCL12 overexpression in electroporated limbs (Fig. 9Aj, k) when compared to controls (Fig. 9Ai). These results show that CXCL12 overexpression in CT enhances ß1integrin activation at MTJ and CXCR7 expression in muscle.

To investigate the effect of ß1integrin activation and CXCR7 expression on myoblast fusion, we first stimulated integrin activation with phorbol-myristate-acetate (PMA) or Mn2+ treatments in myoblast cultures. Both treatments are known to activate integrins with Mn2+ changing the external conformation of integrins in the absence of a bound ligand (Outside-in mechanism) while PMA, by PKC stimulation, allows Talin to activate the cytoplasmic tail of integrins (Inside-out mechanism), (Ye et al., 2012). Foetal myoblasts were submitted to PMA or Mn2+ treatments for 24 hours and 3 hours respectively. As expected, TASC immunostaining revealed a strong integrin activation in enlarged myotubes of PMA treated cultures (Fig. 9Bf) and an increase in CXCR7 expression (Fig. 9Bj) when compared to controls (Fig. 9Be, i). Integrin activation induced by PMA treatment leaded to a massive myoblast fusion (Fig. 9Bb-j), illustrated by an increase of the fusion index when compared to controls (Fig. 9Bk), with large myotubes containing many grouped myonuclei (Fig. 9Bb) compared to the well-aligned myonuclei in control myotubes (Fig. 9Ba). Integrin activation by Mn2+ treatment in cultures also increased myoblast fusion and CXCR7 expression (Supp. Fig. 6a-d). We conclude that ß1integrin activation increases CXCR7 expression and activates myoblast fusion.

To determine if integrin activation induced myoblast fusion via CXCR7, we blocked CXCR7 function in integrin-activated myoblast cultures. Foetal myoblasts were transfected with RCAS-*dnCXCR7* and treated with PMA or Mn2+ to activate integrins. We found that the fusion phenotype induced by integrin activation (Fig. 9Bb, f, j, k) was not observed in PMA-treated cultures transfected with *dnCXCR7* (Fig. 9Bd, h, k), which exhibited a fusion index similar to that of *dnCXCR7*-transfected cultures (Fig. 9Bk), which, as expected, presented a reduced myoblast fusion (Fig. 9Bc, g, k). Similar results were obtained with Mn2+ treatment on *dnCXCR7*-transfected cultures (Supp. Fig. 6e, f). These results demonstrate that the blockade of CXCR7 function prevented the fusion effect of integrin activation.

Taken together, our data show that CXCL12, expressed in limb CT and known to promote CT markers and extracellular matrix components (Nassari et al., 2017), increases ß1integrin

activation at the MTJ and CXCR7 expression at muscle tips, which in turn, promotes myoblast fusion. Finally, we analyzed whether the addition of CXCL12 on myoblast cultures, which does not promote myoblast fusion, has an effect on ß1integrin activation and CXCR7 expression and showed that adding CXCL12 on foetal myoblasts *in vitro* did not change ß1integrin activation and CXCR7 expression (Supp. Fig. 7), confirming that CXCL12 does not act directly via binding to CXCR7 receptor to activate myoblast fusion in chicken limb muscles.

Discussion

In this study, we show that *CXCR7*, a CXCL12 chemokine receptor, exhibits a restricted expression at the tips of muscle fibers, exclusive from the central location of *TMEM8C* during chicken limb foetal myogenesis. CXCR7 promotes myoblast fusion independently of the muscle specific *TMEM8C* fusion gene, by cooperating with EGFR signalling. We also show that CXCL12 ligand mimics indirectly the CXCR7 fusion effect, by increasing ß1integrin activation at the MTJ and CXCR7 expression at muscle tips.

CXCR7 function on myoblast fusion is not related to those of other myofiber tips markers

CXCR7 displays a regionalized expression at muscle tips close to tendon in limb foetal muscles. The molecular specificity of muscle tips facing the tendon has been first highlighted by the localized expression of signalling pathways during development of this region in chicken. FGF and BMP pathways have been shown to be restricted at the tips of foetal myofibers (Edom-Vovard et al., 2001; Wang et al., 2010). However, the deregulation of FGF and BMP pathways in chicken limbs leads to different phenotypes to that of CXCR7 (Figs. 2, 3). FGF4 has been shown to promote the formation of tendon CT at the expense of myogenic cells (Edom-Vovard et al., 2001); (Edom-Vovard et al., 2002), while BMP increases the number of muscle progenitors at the expense of muscle CT in chicken limbs during foetal development (Esteves de Lima et al., 2021). The fusion phenotype of CXCR7 in myoblast cultures (Fig. 4) is also not mimicked by BMP and FGF, since both factors are recognized as potent inhibitors of muscle differentiation *in vitro* (Lathrop et al., 1985; Ono et al., 2011; Pizette et al., 1996). These phenotypes in chicken limb muscles and myoblast cultures lead us to conclude that FGF and BMP signalling are not directly involved in the CXCR7-promoting fusion effect at muscle tips. LoxL3 (Lysyl-oxidase-Like-3) enzyme, known to remodel the

extracellular matrix, has also been shown to be specifically localized at the myofiber tips and to regulate integrin-mediated signalling at muscle attachment sites (Kraft-Sheleg et al., 2016) but LoxL3 mutant mouse displays abnormal myofiber anchorage at the MTJ (Kraft-Sheleg et al., 2016), a phenotype not related to myoblast fusion. Finally, analysis of single-nucleus RNA-sequencing data in post-natal and adult muscles have identified a specific transcriptional signature in myonuclei at the MTJ compartment (Chemello et al., 2020; Dos Santos et al., 2020; Kim et al., 2020; Petrany et al., 2020). However, CXCR7 has not been pinpointed in these data, underlying the possibility that it is only required for myoblast fusion during the establishment of the MTJ and down-regulated at post-natal stages.

A CXCR7/EGFR-dependent fusion mechanism occurs at the tips of foetal muscles

We show that CXCR7 effect on myoblast fusion requires EGFR signaling in cell cultures. The requirement of EGFR signalling for CXCR7 function has been already shown in normal and tumor prostate epithelial cells, in which CXCR7 induces EGFR phosphorylation/activation in a CXCR7 ligand–independent fashion, through a physical association of CXCR7 with EGFR that is regulated by ß-arrestin (Kallifatidis et al., 2016; Salazar et al., 2014; Singh and Lokeshwar, 2011). Interestingly, both *Cxcr7* and *Egfr* genes were identified in a siRNA screen performed on mouse myogenic C2C12 cells to determine genes involved in myoblast fusion (Melendez et al., 2021). In human muscle cell cultures, it has been shown that EGFR activity is down-regulated during myogenesis and that this event is required for muscle differentiation (Leroy et al., 2013). However, EGFR phosphorylation is increased during muscle differentiation in C2C12 muscle cell line (Horikawa et al., 1999) and EGFR activation rescues regeneration defects in dystrophic muscle (Wang et al., 2019). In addition, β-arrestin has been shown to be essential in human myoblasts for cell cycle exit and myoblast fusion through EGFR activation (Santos-Zas et al., 2016) and ß-arrestin is a well-known CXCR7 intracellular relay (Rajagopal et al., 2010). Interestingly, CXCR7 has been shown to activate EGFR independently of both CXCR7 and EGFR ligands (Kallifatidis et al., 2016; Moro et al., 2002; Singh and Lokeshwar, 2011), suggesting that CXCR7/EGFR-dependent myoblast fusion would operate independently of direct binding of ligands.

CXCL12-dependent ECM-integrin interactions are involved in myoblast fusion via CXCR7

We found that CXCL12 overexpression in CT mimics the fusion phenotype observed with the gain-of-function of CXCR7 receptor in limb muscles *in vivo*. In addition, CXCL12

443 overexpression in CT enhances ß1integrin activation at the MTJ and CXCR7 expression at
444 muscle tips (Fig. 9). As addition of CXCL12 to cultures of foetal myoblasts expressing
445 CXCR7 has no effect on myoblast fusion and no effect on ß1integrin activation and CXCR7
446 expression, we suggest that the CXCL12-dependent fusion effect does not result from a direct
447 binding of CXCL12 to CXCR7 but from the positive action of CXCL12 on extracellular
448 matrix which would enhance ß1integrin activation at the MTJ and increase CXCR7
449 expression at muscle tips, resulting in myoblast fusion. Consistent with this hypothesis are our
450 data showing that CXCL12 transcripts in chicken limb are strongly expressed around
451 CXCR4-expressing vessels and faintly near MTJs where CXCR7 expression is observed (Fig.
452 1). We also previously showed that CXCL12 overexpression in limb CT promotes the
453 expression of CT markers and extracellular matrix genes by altering vascular network via
454 binding to CXCR4 and not to CXCR7 (Nassari et al., 2017). In addition, CXCR7 expression
455 is closely associated with muscle tips at the MTJ, where integrins are specifically enriched
456 and have been shown to participate in myoblast fusion both *in vitro* and *in vivo* (McClure et
457 al., 2019; Quach et al., 2009; Schwander et al., 2003). We show that myoblast fusion induced
458 by ß1integrin activation in cultures requires CXCR7 (Fig. 6), putting CXCR7 downstream of
459 ß1integrin activation at MTJ. Finally, EGFR signalling can be transactivated by integrins
460 independently of EGFR ligand (Moro et al., 2002), leading to the possible scenario that
461 ß1integrins could induce CXCR7/EGFR transactivation and myoblast fusion independently of
462 a direct binding of CXCR7 to CXCL12 ligand. However, the question remains why CXCL12
463 would be unable to bind CXCR7. One possibility could be that most CXCL12 would be
464 trapped by the neighboring CXCR4-expressing endothelial cells. Alternatively, it has been
465 shown that glycosaminoglycans are crucial partners in CXCL12 presentation to CXCR4
466 receptor (Panitz et al., 2016), underlying the possibility that CXCL12 in limb mesenchyme
467 interacts with proteoglycans, favoring its binding to CXCR4 at the expense of CXCR7.
468
469 **A TMEM8C-independent/CXCR7-dependent fusion mechanism occurs at the tips of**
470 **foetal muscles**
471 Numerous transmembrane proteins have been involved in myoblast fusion (Demonbreun et
472 al., 2015) but to date, only MYOMAKER (TMEM8C in chicken) has been described to be
473 muscle specific during developmental and regenerative myogenesis (Petrany and Millay,
474 2019). We identified CXCR7 as a novel transmembrane protein involved in foetal myoblast
475 fusion in chicken limbs and myoblast cultures (Figs. 3, 4, 6). However, the expression of
476 *CXCR7* transcripts at muscle tips is exclusive to that of *TMEM8C* mainly located centrally

(Fig. 4, Esteves de Lima et al., 2022). The mutually exclusive expression of *CXCR7* and *TMEM8C* transcripts and the fact that *TMEMC8* expression is not modified in *CXCR7* gain- and loss-of -function experiments in chicken limbs and myoblast cultures (Figs. 3, 4, 6) indicate that myoblast fusion occurs at muscle tips independently of *TMEM8C*. This is confirmed by the results showing that *CXCR7* can modulate myoblast fusion *in vitro* in the absence of functional *TMEM8C*. Although MYOMAKER is a critical factor for myoblast fusion and muscle formation (Millay, 2022), some MYOMAKER-independent fusion pathways have been already reported. Complete defective myoblast fusion is not observed in *Myomaker* mutant in fish (Shi et al., 2018) and inactivation of *Myomaker* in fibroblast-derived myonuclei at the MTJ has no effect on their fusion capacity (Yaseen et al., 2021). Similarly, fusion index is increased in co-cultures of human tenocytes and myoblasts without any change in *Myomaker* expression (Tsuchiya et al., 2022). These data support our observations that other factors can control the fusion mechanisms at the muscle tips. Our observations suggest two different types of fusion within foetal muscles, one located at myofiber tips and the other one in central regions of muscles. The reasons for these two fusion mechanisms remain elusive, but one can speculate that it is related to the spindle shape of the growing muscle, with a large diameter in the central region compared to the tips. TMEM8C-dependent fusion in the muscle bulk would support growth in diameter while CXCR7-dependent fusion at the tips would support growth in length or elongation. Consistent with this hypothesis are the observations that CXCR7 misregulation has an effect on myofiber length (Figs. 2, 3, 4, 8) and that reducing the number of myonuclei by MYOMAKER inactivation in satellite cells during post-natal muscle growth in mice leads mostly to the reduction in muscle diameter and volume rather than myofiber length (Cramer et al., 2020).

In summary, we propose a model in which ß1integrin activation at the MTJ would lead to the interaction of CXCR7 receptor with the EGF receptor to promote myoblast fusion specifically at the tips of muscle fibers and independently of the muscle-specific fusion gene *TMEM8C* (Fig. 10). CXCL12, expressed in CT, would participate indirectly to this process by regulating extracellular matrix genes and ß1integrin activation at the MTJ. This molecular network would enable muscle growth and elongation at the tendon/muscle interface.

Acknowledgements

We thank Estelle Hirsinger and Christophe Marcelle for critical reading of the manuscript. We thank Wen Luo for the gift of siTMEM8C primers.

Competing interests

The authors declare no competing or financial interests.

Material and methods

Chick embryos

Fertilized chick eggs from commercial sources (JA 57 strain, Institut de Sélection Animale, Lyon, France, and White Leghorn, HAAS, Strasbourg) were incubated at 38°C in a humidified incubator until appropriate stages. Embryos were staged according to the number of days in ovo (E).

Constructs

The chicken *CXCL12, dnCXCR7* and *CXCR7* coding regions were amplified by PCR from a RT-PCR-derived cDNA library made from E5 chick limb, using primers containing the ClaI enzyme restriction site. The *dnCXCR7* coding region is a truncated form of *CXCR7* lacking the C-terminal part of the sequence ((Ray et al., 2013)). Amplified *dnCXCR7* and *CXCR7* sequences were inserted into pCR-II TOPO vector using TOPO-TA cloning kit (InVitrogen) or pGEM vector using pGEM-T easy vector system kit (Promega). Inserted sequences were excised by digestion with ClaI and inserted into the ClaI site of the replication-competent retroviral vector RCASBP(A), ((Hughes et al., 1987)), previously digested with ClaI enzyme. Clones containing the *dnCXCR7* or *CXCR7* coding regions in the sense orientation were selected. For pT2AL-CMV/Tomato-T2A-CXCL12 construct, the chicken *CXCL12* coding sequence was amplified by PCR from a RT-PCR-derived cDNA library made from E5 chick limb, using a forward primer containing the BstbI enzyme restriction site and a reverse primer comprising the PmlI enzyme restriction site. Purified PCR products were included into the PCR-II TOPO vector using TOPO-TA cloning kit (InVitrogen), and clones containing *CXCL12* sequence with BstbI and PmlI restriction sites respectively in 5' and 3' ends of the coding sequence were selected. The TOPO/BstbI-CXCL12-PmlI and TOPO/BstbI-CXCL14-PmlI were then digested with BstbI and PmlI enzymes. Purified digested products were finally inserted into the PT2AL-CMV/Tomato-T2A-GFP plasmid, from which GFP was previously extracted by BstbI and PmlI enzymatic digestion and clones containing *CXCL12* coding sequence were selected.

Primary muscle cell cultures

Forelimbs of E10 chicken embryos were used to establish primary myoblast cultures as previously described ((Havis et al., 2012)). Limb muscles were cut in small pieces in Minimal Essential Medium (MEM) followed by mechanical dissociation. Homogenate was then centrifuged and the supernatant was filtered into a 40µm filter to collect muscle cells. Centrifugation and filtration steps were repeated several times. Chicken myoblasts were plated on a 0,1% gelatin coated plastic dish in MEM complemented with 10% of foetal calf serum for proliferation conditions during 48 hours. For differentiation conditions, MEM was complemented with 2% of foetal calf serum and cells cultured for 3 or 5 more days. Primary myoblasts were transfected at around 30-40% confluence with the Calcium Phosphate transfection kit (Invitrogen). To control the effect of CXCL12 supernatant collected from infected chicken fibroblasts in vitro, its chemotactic effect was tested on chicken fibroblast cultures in a Boyden chamber. To confirm the effect of CXCL12 supernatant, some cultures were conducted in N2 minimum medium without serum (R&D System) and recombinant CXCL12 protein (R&D System) was added at 50ng/ml. For pharmacological experiments, primary myoblasts were transfected at around 30-40% confluence, cultured in proliferation medium until confluence and treated with pharmacological agents after being transferred into differentiation medium. For experiments testing ß1integrin activation, PMA (Sigma Merck, 5µg/ml) or Manganese Chloride (Sigma Merck, 2mM) was added to proliferating myoblasts for 24 hours or 3 hours respectively. For experiments testing the implication of the phosphorylated form of EGF receptor, PD15035 inhibitor (Sigma Merck, 6µm) was added to proliferating myoblasts for 1 hour.

Myoblast migration assay

Migration of myoblasts was analysed using scratch wound healing assay. Briefly, control and transfected cells were plated in the culture dish without gelatin and cultured until they reached 90% of confluency. Cells were scratched from the plate using a plastic tip to create the wound. The wound healing manifested by the ability of the cells to refill the created gap was monitored after 48h of culture.

Production and grafting of recombinant RCAS-expressing cells

Primary chicken fibroblasts were transfected with RCAS-*CXCR7*, RCAS-*dnCXCR7* or empty RCAS as a control, using Calcium Phosphate transfection kit (InVitrogen) and grown for one week. One day before grafting, transfected fibroblasts were plated into bacteria plastic dishes

in order to induce cell aggregate formation. Pellets of approximately 50 µm in diameter were grafted into the right wing bud of E4 chick embryos. Embryos were harvested at various times after grafting and processed for whole mount or section staining or RT-q-PCR. The left wing was used as an internal control. Owing to certain variability in virus spread among embryos, the ectopic gene expression was systematically checked by in situ hybridization.

Lateral plate mesoderm electroporation

E2.5 chicken embryos were electroporated as previously described ((Bourgeois et al., 2015)). PT2AL-CMVCXCL12 (1.5-2 µg/µl) construct was mixed with the transposase vector CMV-T2TP (molar ratio 1/3) to allow stable integration of genes in the chicken genome, in a solution containing 0.33% carboxymethyl cellulose, 1% Fast green, 1mM $MgCl_2$ in PBS. DNA mix was injected with a glass capillary in the coelomic cavity between somatopleural and splanchnopleural mesoderm, at the level of the forelimb territory. Homemade platinum electrodes were placed above and below the embryos, with the negative electrode inserted into the yolk and the positive electrode localized above the presumptive forelimb region. Electroporation was delivered using a Nepagene NEPA21 electroporator using the following parameters: 2 pulses of 70V, 1ms duration with 100 ms interpulse interval followed by 5 pulses of 40V, 2ms duration with 500 ms interpulse interval.

In situ hybridization and immunostaining to tissue sections and cultures

Forelimbs were fixed in a 4% paraformaldehyde solution in PBS, successively embedded in a 4% and 15% sucrose solution, and then frozen in chilled isopentane. Cryostat-cut sections of 12-20 µm were collected on Superfrost/Plus slides (CML, France). Immunostaining and in situ hybridization were proceeded as previously described ((Escot et al., 2013)). For grafted and electroporated embryos, the electroporated and control forelimbs from the same embryo were embedded together in order to allow comparison. For in situ hybridization, the following digoxigenin-labeled mRNA probes were used: chicken *CXCL12* ((Escot et al., 2013)), chicken *CXCR7* ((Escot et al., 2013)). The chicken *TMEM8C (MYOMAKER)* probe was produced from a RT-PCR-derived cDNA library made from chicken primary muscle cell cultures. In some cases, fluorescent in situ hybridization was performed according to (Wilmerding et al., 2022)). For immunostaining, the following primary antibodies were used: anti-myosin MF20 (Developmental Studies Hybridoma Bank, non-diluted supernatant), anti-CXCR4 (1:1000, (Escot et al., 2013)), anti-CXCR7 (1:200, Abcam), anti-MEP21 (1:200, generous gift from T. Jaffredo), anti-PAX7 (1:200, Developmental Studies Hybridoma Bank),

anti-MYOGENIN (1:200, generous gift from C. Marcelle), anti-activated ß1 integrin TASC (1:100, Millipore), anti-phospho EGFR Tyr-1068 (1:100, In Vitrogen). Proliferation analysis (EdU) was performed using the Click-iT kit (Thermo Fisher Scientific, France) or the anti-phospho-histone-3 antibody (1:1000, Upstate Biotechnology). Immunolabelings were performed using secondary antibodies conjugated to Alexa Fluor 488 and 555 (InVitrogen). Nuclei were stained using DAPI (1:1000, Sigma). Stained tissue sections and cultures were observed with an inverted Leica microscope, images were collected with the Leica software and processed using Adobe Photoshop software.

3D reconstructions of muscles

Grafted and control forelimbs were immunostainned in toto for MF20. Whole-mount immunostained forelimbs were imaged with a Zeiss biphoton microscope and generated files were analysed with the IMARIS software (Bitplane) to perform 3D muscle reconstructions. Reconstructed images were then processed using Adobe Photoshop software.

RNA isolation, reverse transcription and quantitative real-time PCR

Total RNAs were extracted from chick limbs or muscle cell cultures using the RNeasy mini kit from Qiagen. 500ng to 1µg RNAs were reverse-transcribed using the High Capacity Retrotranscription kit (Applied Biosystems). RT-qPCR was performed using SYBR Green PCR Master Mix (Applied Biosystems). Primer sequences used for TMEMC8 were the following: Forward 5'-TGGGGTGTCCCTGATGGC-3', Reverse 5'-CCCGATGGGTCCTAGTAG-3'. The relative mRNA levels were calculated using the 2^-ΔΔCt method ((Livak and Schmittgen, 2001)). The ΔCts were obtained from Ct normalized with chick *S17* levels in each sample. Each sample was analyzed in duplicate. Results were expressed as Standard Deviation (SD). Statistical analysis was performed with Graphpad Prism V6 software using the non-parametric Mann-Whitney test to determine p-values. Statistical significance was set at $p<0.05$.

Quantification and statistical analyses

For enumeration of myoblasts and myotubes in vitro, pictures of cultures stained with PAX7, MYOG and MF20 antibodies were assembled and counted. MYOG-positive nuclei were counted outside and inside the MF20-positive myotubes. Myoblast fusion was estimated by counting the number of DAPI-positive nuclei inside the MF20-positive myotube compared to the total number of DAPI-positive nuclei. Proliferation was quantified by estimating the

number of EDU-positive cells among the total number of DAPI-positive nuclei. Results shown are the mean of at least six biological samples coming from at least three independent cultures. Quantification in vivo was realized on transverse sections of control, grafted and electroporated limbs immunostained with PAX7, MYOG or MF20 antibodies. Muscle area measurement and determination of the number of PAX7-positive cells and MYOG-positive nuclei were performed on five to eight successive sections of five different muscles in four to six different embryos. The number of PAX7-positive cells and MYOG-positive nuclei was estimated on the total number of DAPI-positive nuclei and compared between experimental and control muscles. Proliferation was quantified by estimating the number of PH3-positive cells among the total number of DAPI-positive nuclei or among the total number of PAX7-positive nuclei. Results shown are the mean of quantification on all sections for each muscle. Quantification analysis was realized with the Cell Counter plug-in of the free software Fidji (Rasband,W.S., ImageJ,U.S.National Institute of Health, Bethesda, Maryland,USA, http://imagej.nih. gov/ij/, 1997–2012). Statistical analysis was performed with Graphpad Prism V6 software using the non-parametric Mann-Whitney test to determine p-values. Statistical significance was set at $p<0.05$.

Bibliography

Abmayr, S. M. and Pavlath, G. K. (2012). Myoblast fusion: Lessons from flies and mice. *Development* **139**, 641–656.

Bae, G.-U., Gaio, U., Yang, Y.-J., Lee, H.-J., Kang, J.-S. and Krauss, R. S. (2008). Regulation of myoblast motility and fusion by the CXCR4-associated sialomucin, CD164. *J. Biol. Chem.* **283**, 8301–9.

Besse, L., Sheeba, C. J., Holt, M., Labuhn, M., Wilde, S., Feneck, E., Bell, D., Kucharska, A. and Logan, M. P. O. (2020). Individual Limb Muscle Bundles Are Formed through Progressive Steps Orchestrated by Adjacent Connective Tissue Cells during Primary Myogenesis. *Cell Rep.* **30**, 3552–3565.e6.

Biressi, S., Tagliafico, E., Lamorte, G., Monteverde, S., Tenedini, E., Roncaglia, E., Ferrari, S., Ferrari, S., Cusella-De Angelis, M. G., Tajbakhsh, S., et al. (2007). Intrinsic phenotypic diversity of embryonic and fetal myoblasts is revealed by genome-wide gene expression analysis on purified cells. *Dev. Biol.* **304**, 633–651.

Bourgeois, A., Esteves de Lima, J., Charvet, B., Kawakami, K., Stricker, S. and Duprez, D. (2015). Stable and bicistronic expression of two genes in somite- and lateral plate-derived tissues to study chick limb development. *BMC Dev. Biol.* **15**, 39.

Buckingham, M. and Rigby, P. W. J. (2014). Gene Regulatory Networks and Transcriptional Mechanisms that Control Myogenesis. *Dev. Cell*.

Chemello, F., Wang, Z., Li, H., McAnally, J. R., Liu, N., Bassel-Duby, R. and Olson, E. N. (2020). Degenerative and regenerative pathways underlying Duchenne muscular dystrophy revealed by single-nucleus RNA sequencing. *Proc. Natl. Acad. Sci. U. S. A.* **117**, 29691–29701.

Comai, G. and Tajbakhsh, S. (2014). Molecular and cellular regulation of skeletal myogenesis. In *Current Topics in Developmental Biology*, pp. 1–73.

Cramer, A. A. W., Prasad, V., Eftestøl, E., Song, T., Hansson, K. A., Dugdale, H. F., Sadayappan, S., Ochala, J., Gundersen, K. and Millay, D. P. (2020). Nuclear numbers in

690 syncytial muscle fibers promote size but limit the development of larger myonuclear domains.
691 *Nat. Commun.* **11**, 1–14.
692 **de Lima, J. E., Bonnin, M. A., Birchmeier, C. and Duprez, D.** (2016). Muscle contraction is
693 required to maintain the pool of muscle progenitors via yap and notch during fetal myogenesis.
694 *Elife* **5**, 1–25.
695 **Demonbreun, A. R., Biersmith, B. H. and McNally, E. M.** (2015). Membrane fusion in muscle
696 development and repair. *Semin. Cell Dev. Biol.* **45**, 48–56.
697 **Dos Santos, M., Backer, S., Saintpierre, B., Izac, B., Andrieu, M., Letourneur, F., Relaix, F.,**
698 **Sotiropoulos, A. and Maire, P.** (2020). Single-nucleus RNA-seq and FISH identify coordinated
699 transcriptional activity in mammalian myofibers. *Nat. Commun.* **11**,.
700 **Edom-Vovard, F., Bonnin, M. a and Duprez, D.** (2001). Misexpression of Fgf-4 in the chick limb
701 inhibits myogenesis by down-regulating Frek expression. *Dev. Biol.* **233**, 56–71.
702 **Edom-Vovard, F., Schuler, B., Bonnin, M.-A., Teillet, M.-A. and Duprez, D.** (2002). Fgf4
703 positively regulates scleraxis and tenascin expression in chick limb tendons. *Dev. Biol.* **247**, 351–
704 366.
705 **Eigler, T., Zarfati, G., Amzallag, E., Sinha, S., Segev, N., Zabary, Y., Zaritsky, A., Shakked, A.,**
706 **Umansky, K. B., Schejter, E. D., et al.** (2021). ERK1/2 inhibition promotes robust myotube
707 growth via CaMKII activation resulting in myoblast-to-myotube fusion. *Dev. Cell* **56**, 3349–
708 3363.e6.
709 **Escot, S., Blavet, C., Härtle, S., Duband, J.-L. and Fournier-Thibault, C.** (2013). Misregulation of
710 SDF1-CXCR4 signaling impairs early cardiac neural crest cell migration leading to conotruncal
711 defects. *Circ. Res.* **113**, 505–16.
712 **Esteves de Lima, J. and Relaix, F.** (2021). Master regulators of skeletal muscle lineage development
713 and pluripotent stem cells differentiation. *Cell Regen.* **10**,.
714 **Esteves de Lima, J., Blavet, C., Bonnin, M. A., Hirsinger, E., Comai, G., Yvernogeau, L., Delfini,**
715 **M. C., Bellenger, L., Mella, S., Nassari, S., et al.** (2021). Unexpected contribution of
716 fibroblasts to muscle lineage as a mechanism for limb muscle patterning. *Nat. Commun.* **12**,.
717 **Esteves de Lima, J., Blavet, C., Bonnin, M.-A., Hirsinger, E., Havis, E., Relaix, F. and Duprez,**
718 **D.** (2022). TMEM8C-mediated fusion is regionalized and regulated by NOTCH signalling
719 during foetal myogenesis. *Development* **149**,.
720 **Fry, D. W., Kraker, A. J., McMichael, A., Ambroso, L. A., Nelson, J. M., Leopold, W. R.,**
721 **Connors, R. W. and Bridges, A. J.** (1994). A specific inhibitor of the epidermal growth factor
722 receptor tyrosine kinase. *Science (80-.).* **265**, 1093–1095.
723 **Ganassi, M., Badodi, S., Ortuste Quiroga, H. P., Zammit, P. S., Hinits, Y. and Hughes, S. M.**
724 (2018). Myogenin promotes myocyte fusion to balance fibre number and size. *Nat. Commun.* **9**,.
725 **García-Andrés, C. and Torres, M.** (2010). Comparative expression pattern analysis of the highly
726 conserved chemokines SDF1 and CXCL14 during amniote embryonic development. *Dev. Dyn.*
727 **239**, 2769–77.
728 **Ge, Y., Waldemer, R. J., Nalluri, R., Nuzzi, P. D. and Chen, J.** (2013). RNAi screen reveals
729 potentially novel roles of cytokines in myoblast differentiation. *PLoS One* **8**, e68068.
730 **Gerrits, H., van Ingen Schenau, D. S., Bakker, N. E. C., van Disseldorp, A. J. M., Strik, A.,**
731 **Hermens, L. S., Koenen, T. B., Krajnc-Franken, M. a M. and Gossen, J. a** (2008). Early
732 postnatal lethality and cardiovascular defects in CXCR7-deficient mice. *Genesis* **46**, 235–45.
733 **Girardi, F., Taleb, A., Ebrahimi, M., Datye, A., Gamage, D. G., Peccate, C., Giordani, L., Millay,**
734 **D. P., Gilbert, P. M., Cadot, B., et al.** (2021). TGFβ signaling curbs cell fusion and muscle
735 regeneration. *Nat. Commun.* **12**,.
736 **Griffin, C. a, Apponi, L. H., Long, K. K. and Pavlath, G. K.** (2010). Chemokine expression and
737 control of muscle cell migration during myogenesis. *J. Cell Sci.* **123**, 3052–60.
738 **Hasty, P., Bradley, a, Morris, J. H., Edmondson, D. G., Venuti, J. M., Olson, E. N. and Klein,**
739 **W. H.** (1993). Muscle deficiency and neonatal death in mice with a targeted mutation in the
740 myogenin gene. *Nature* **364**, 501–506.
741 **Havis, E., Coumailleau, P., Bonnet, A., Bismuth, K., Bonnin, M. A., Johnson, R., Fan, C. M.,**
742 **Relaix, F., Shi, D. L. and Duprez, D.** (2012). Sim2 prevents entry into the myogenic program
743 by repressing myod transcription during limb embryonic myogenesis. *Development* **139**, 1910–
744 1920.

Havis, E., Bonnin, M., de Lima, J., Charvet, B., Milet, C. and Duprez, D. (2016). TGFβ and FGF promote tendon progenitor fate and act downstream of muscle contraction to regulate tendon differentiation during chick limb development. *Development* **143**, 3839–3851.

Horikawa, M., Higashiyama, S., Nomura, S., Kitamura, Y., Ishikawa, M. and Taniguchi, N. (1999). Upregulation of endogenous heparin-binding EGF-like growth factor and its role as a survival factor in skeletal myotubes. *FEBS Lett.* **459**, 100–104.

Horsley, V., Jansen, K. M., Mills, S. T. and Pavlath, G. K. (2003). IL-4 acts as a myoblast recruitment factor during mammalian muscle growth. *Cell* **113**, 483–494.

Hughes, S. H., Greenhouse, J. J., Petropoulos, C. J. and Sutrave, P. (1987). Adaptor plasmids simplify the insertion of foreign DNA into helper-independent retroviral vectors. *J. Virol.* **61**, 3004–12.

Hunger, C., Ödemis, V. and Engele, J. (2012). Expression and function of the SDF-1 chemokine receptors CXCR4 and CXCR7 during mouse limb muscle development and regeneration. *Exp. Cell Res.* **318**, 2178–90.

Kallifatidis, G., Munoz, D., Singh, R. K., Salazar, N., Hoy, J. J. and Lokeshwar, B. L. (2016). β-Arrestin-2 counters CXCR7-mediated EGFR transactivation and proliferation. *Mol. Cancer Res.* **14**, 493–503.

Kardon, G. (1998). Muscle and tendon morphogenesis in the avian hind limb. *Development* **125**, 4019–4032.

Kim, M., Franke, V., Brandt, B., Lowenstein, E. D., Schöwel, V., Spuler, S., Akalin, A. and Birchmeier, C. (2020). Single-nucleus transcriptomics reveals functional compartmentalization in syncytial skeletal muscle cells. *Nat. Commun.* **11**, 1–14.

Kiss, D. L., Windus, L. C. E. and Avery, V. M. (2013). Chemokine receptor expression on integrin-mediated stellate projections of prostate cancer cells in 3D culture. *Cytokine* **64**, 122–130.

Koch, C. and Engele, J. (2020). Functions of the CXCL12 receptor ACKR3/CXCR7-what has been perceived and what has been overlooked. *Mol. Pharmacol.* **98**, 577–585.

Kraft-Sheleg, O., Zaffryar-Eilot, S., Genin, O., Yaseen, W., Soueid-Baumgarten, S., Kessler, O., Smolkin, T., Akiri, G., Neufeld, G., Cinnamon, Y., et al. (2016). Localized LoxL3-Dependent Fibronectin Oxidation Regulates Myofiber Stretch and Integrin-Mediated Adhesion. *Dev. Cell* **36**, 550–561.

Landemaine, A., Rescan, P. Y. and Gabillard, J. C. (2014). Myomaker mediates fusion of fast myocytes in zebrafish embryos. *Biochem. Biophys. Res. Commun.* **451**, 480–484.

Lathrop, B., Olson, E. and Glaser, L. (1985). Control by fibroblast growth factor of differentiation in the BC3H1 muscle cell line. *J. Cell Biol.* **100**, 1540–1547.

Leroy, M. C., Perroud, J., Darbellay, B., Bernheim, L. and Konig, S. (2013). Epidermal Growth Factor Receptor Down-Regulation Triggers Human Myoblast Differentiation. *PLoS One* **8**,.

Livak, K. J. and Schmittgen, T. D. (2001). Analysis of relative gene expression data using real-time quantitative PCR and. *Methods* **25**, 402–408.

Luo, W., Li, E., Nie, Q. and Zhang, X. (2015). Myomaker, regulated by MYOD, MYOG and miR-140-3P, promotes chicken myoblast fusion. *Int. J. Mol. Sci.* **16**, 26186–26201.

Martin-Bermudo, M. D. (2000). Integrins modulate the Egfr signaling pathway to regulate tendon cell differentiation in the Drosophila embryo. *Development* **127**, 2607–2615.

Mayer, U., Saher, G., Fassler, R., Bornemann, A., Echtermeyer, F., Von der Mark, H., Miosge, N., Poschi, E. and Von der Mark, K. (1997). Absence of integrin alpha 7 causes a novel form of muscular dystrophy. *Nat. Genet.* **17**, 318–323.

McClure, M. J., Ramey, A. N., Rashid, M., Boyan, B. D. and Schwartz, Z. (2019). Integrin-α7 signaling regulates connexin 43, M-cadherin, and myoblast fusion. *Am. J. Physiol. - Cell Physiol.* **316**, C876–C887.

Melchionna, R., Di Carlo, A., De Mori, R., Cappuzzello, C., Barberi, L., Musarò, A., Cencioni, C., Fujii, N., Tamamura, H., Crescenzi, M., et al. (2010). Induction of myogenic differentiation by SDF-1 via CXCR4 and CXCR7 receptors. *Muscle Nerve* **41**, 828–35.

Melendez, J., Sieiro, D., Salgado, D., Morin, V., Dejardin, M. J., Zhou, C., Mullen, A. C. and Marcelle, C. (2021). TGFβ signalling acts as a molecular brake of myoblast fusion. *Nat. Commun.* **12**, 1–11.

Millay, D. P., O'Rourke, J. R., Sutherland, L. B., Bezprozvannaya, S., Shelton, J. M., Bassel-

duby, R. and Olson, E. N. (2013). Myomaker:a membrane activator of myoblast fusion and muscle formation. *Nature* **499**, 301–305.

Moro, L., Dolce, L., Cabodi, S., Bergatto, E., Erba, E. B., Smeriglio, M., Turco, E., Retta, S. F., Giuffrida, M. G., Venturino, M., et al. (2002). Integrin-induced epidermal growth factor (EGF) receptor activation requires c-Src and p130Cas and leads to phosphorylation of specific EGF receptor tyrosines. *J. Biol. Chem.* **277**, 9405–9414.

Nassari, S., Blavet, C., Bonnin, M.-A., Stricker, S., Duprez, D. and Fournier-Thibault, C. (2017). The chemokines CXCL12 and CXCL14 differentially regulate connective tissue markers during limb development. *Sci. Rep.* **7**,.

Neugebauer, K. M. and Rekhart, L. F. (1991). Cell-surface regulation of ß1-integrin activity on developing retinal neurons. *Nature* **350**, 68–71.

Ono, Y., Calhabeu, F., Morgan, J. E., Katagiri, T., Amthor, H. and Zammit, P. S. (2011). BMP signalling permits population expansion by preventing premature myogenic differentiation in muscle satellite cells. *Cell Death Differ.* **18**, 222–234.

Panitz, N., Theisgen, S., Samsonov, S. A., Gehrcke, J. P., Baumann, L., Bellmann-Sickert, K., Köhling, S., Teresa Pisabarro, M., Rademann, J., Huster, D., et al. (2016). The structural investigation of glycosaminoglycan binding to CXCL12 displays distinct interaction sites. *Glycobiology* **26**, 1209–1221.

Petrany, M. J. and Millay, D. P. (2019). Cell Fusion: Merging Membranes and Making Muscle. *Trends Cell Biol.* **29**, 964–973.

Petrany, M. J., Swoboda, C. O., Sun, C., Chetal, K., Chen, X., Weirauch, M. T., Salomonis, N. and Millay, D. P. (2020). Single-nucleus RNA-seq identifies transcriptional heterogeneity in multinucleated skeletal myofibers. *Nat. Commun.* **11**,.

Pizette, S., Coulier, F., Birnbaum, D. and Delapeyrière, O. (1996). FGF6 modulates the expression of fibroblast growth factor receptors and myogenic genes in muscle cells. *Exp. Cell Res.* **224**, 143–151.

Quach, N., Biressi, S., Reichardt, L., Keller, C. and Rando, T. (2009). Focal adhesion kinase signaling regulates the expression of caveolin 3 and ß1 integrin, genes essential for normal myoblast fusion. *Mol. Biol. Cell* **20**, 3422–3435.

Rajagopal, S., Kim, J., Ahn, S., Craig, S., Lam, C. M., Gerard, N. P., Gerard, C. and Lefkowitz, R. J. (2010). Beta-arrestin- but not G protein-mediated signaling by the "decoy" receptor CXCR7. *Proc. Natl. Acad. Sci. U. S. A.* **107**, 628–32.

Ray, P., Mihalko, L. A., Coggins, N. L., Moudgil, P., Ehrlich, A., Luker, K. E. and Luker, G. D. (2013). Carboxy-terminus of CXCR7 Regulates Receptor Localization and Function. *Int. J. Biochem. cell Biol.* **44**, 669–678.

Rehimi, R., Khalida, N., Yusuf, F., Dai, F., Morosan-Puopolo, G. and Brand-Saberi, B. (2008). Stromal-derived factor-1 (SDF-1) expression during early chick development. *Int. J. Dev. Biol.* **52**, 87–92.

Relaix, F., Rocancourt, D., Mansouri, A. and Buckingham, M. (2004). Divergent functions of murine Pax3 and Pax7 in limb muscle development. *Genes Dev.* **18**, 1088–1105.

Relaix, F., Rocancourt, D., Mansouri, A. and Buckingham, M. (2005). A Pax3/Pax7-dependent population of skeletal muscle progenitor cells. *Nature* **435**, 948–53.

Salazar, N., Muñoz, D., Kallifatidis, G., Singh, R. K., Jordà, M. and Lokeshwar, B. L. (2014). The chemokine receptor CXCR7 interacts with EGFR to promote breast cancer cell proliferation. *Mol. Cancer* **13**, 1–13.

Santos-Zas, I., Gurriarán-Rodríguez, U., Cid-Díaz, T., Figueroa, G., González-Sánchez, J., Bouzo-Lorenzo, M., Mosteiro, C. S., Señarís, J., Casanueva, F. F., Casabiell, X., et al. (2016). β-Arrestin scaffolds and signaling elements essential for the obestatin/GPR39 system that determine the myogenic program in human myoblast cells. *Cell. Mol. Life Sci.* **73**, 617–635.

Schwander, M., Leu, M., Stumm, M., Dorchies, O. M., Ruegg, U. T., Schittny, J. and Müller, U. (2003). B1 Integrins Regulate Myoblast Fusion and Sarcomere Assembly. *Dev. Cell* **4**, 673–685.

Sierro, F., Biben, C., Martinez-Munoz, L., Mellado, M., Ransohoff, R. M., Li, M., Woehl, B., Leung, H., Groom, J., Batten, M., et al. (2007). Disrupted cardiac development but normal hematopoiesis in mice deficient in the second CXCL12 / SDF-1 receptor , CXCR7. *Proc. Natl. Acad. Sci.* **104**, 14759–14764.

Singh, R. K. and Lokeshwar, B. L. (2011). The IL-8-regulated chemokine receptor CXCR7 stimulates EGFR signaling to promote prostate cancer growth. *Cancer Res.* **71**, 3268–3277.

Sotiropoulos, A., Ohanna, M., Kedzia, C., Menon, R. K., Kopchick, J. J., Kelly, P. A. and Pende, M. (2006). Growth hormone promotes skeletal muscle cell fusion independent of insulin-like growth factor 1 up-regulation. *Proc. Natl. Acad. Sci. U. S. A.* **103**, 7315–7320.

Stockdale, F. (1992). Myogenic Cell Lineages. *Dev. Biol.* **154**, 284–298.

Valdivia, M., Vega-Macaya, F. and Olguín, P. (2017). Mechanical control of myotendinous junction formation and tendon differentiation during development. *Front. Cell Dev. Biol.* **5**, 1–8.

Vallecillo-García, P., Orgeur, M., Vom Hofe-Schneider, S., Stumm, J., Kappert, V., Ibrahim, D. M., Börno, S. T., Hayashi, S., Relaix, F., Hildebrandt, K., et al. (2017). Odd skipped-related 1 identifies a population of embryonic fibro-adipogenic progenitors regulating myogenesis during limb development. *Nat. Commun.* **8**,.

Vasyutina, E., Stebler, J., Brand-saberi, B., Schulz, S., Raz, E. and Birchmeier, C. (2005). CXCR4 and Gab1 cooperate to control the development of migrating muscle progenitor cells. 2187–2198.

Wang, H., Noulet, F., Edom-Vovard, F., Le Grand, F. and Duprez, D. (2010). Bmp Signaling at the Tips of Skeletal Muscles Regulates the Number of Fetal Muscle Progenitors and Satellite Cells during Development. *Dev. Cell* **18**, 643–654.

Wang, Y. X., Feige, P., Brun, C. E., Hekmatnejad, B., Dumont, N. A., Renaud, J. M., Faulkes, S., Guindon, D. E. and Rudnicki, M. A. (2019). EGFR-Aurka Signaling Rescues Polarity and Regeneration Defects in Dystrophin-Deficient Muscle Stem Cells by Increasing Asymmetric Divisions. *Cell Stem Cell* **24**, 419–432.e6.

Wilmerding, A., Bouteille, L., Caruso, N., Bidaut, G., Etchevers, H. C., Graba, Y. and Delfini, M.-C. (2022). Sustained experimental activation of FGF8/ERK in the developing chicken spinal cord models early events in ERK-mediated tumorigenesis. *Neoplasia* **24**, 120–132.

Windus, L. C., Glover, T. T. and Avery, V. M. (2014). Bone-stromal cells up-regulate tumourigenic markers in a tumour-stromal 3D model of prostate cancer. *Mol. Cancer* **13**, 1–19.

Ye, F., Kim, C. and Ginsberg, M. H. (2012). Reconstruction of integrin activation. *Blood* **119**, 26–33.

Legends to Figures

Figure 1: CXCR7 receptor is expressed in foetal myogenic cells in chicken embryonic limb. In situ hybridization for *CXCL12* (a, i, p, t), *CXCR7* (c, d, e, h, j, k, o, q, s), *SCX* (r) and immunostaining for CXCR4 (b, d), CXCR7 (f, g, l-n), PAX7 (f, g, m) and MF20 (l, n, o-t) on transverse sections of E5 (a-g), E8 (j-n), E10 (o, p, r, s) and longitudinal section of E8 (h, i) and E10 (q) chicken embryo limbs. At E5, CXCR4+ muscle masses express CXCR7 in a few PAX7+ cells. From E8, CXCR7 was restricted to the tips of MF20+ myotubes, facing the SCX+ MTJ at E10. At all stages, CXCL12 was expressed in CT with a strong expression around limb vessels at E10. Dorsal at the top, posterior at the left, u: ulna, r: radius. Bars: 100 µm in a-c, e, f, j, l, o, p, r-t; 50 µm in d, g, h, i, k, m, n, q.

Figure 2: Misregulation of CXCR7 receptor induces muscle defaults in chicken embryonic limb. (A) Pellets of CEF transfected with RCAS-*CXCR7* or *dnCXCR7* were grafted in the forelimb of E4 chicken embryos. Infected and control (contralateral) limbs were

collected at E10 and analysed. (B, C) Dorsal views of whole mount MF20 immunostaining (Ba, b, Ca, b) revealed differences in muscle patterning between infected limbs (Bb, Cb) and controls (Ba, Ca) confirmed by 3D reconstructions of individual muscles in *dnCXCR7*- (Bd) and *CXCR7*- (Cd) infected limbs when compared to controls (Bc, Cc). Volume and length analysis in reconstructed muscles shown in B and C shows that *dnCXCR7* overexpression induced a decrease in muscle volume and length (Be, f), while *CXCR7* overexpression resulted in an increase in muscle volume and length (Ce, f). Colors of arrows, individual muscles and histograms indicate the same muscle in each condition. ANC: anconeus, EDC: extensor digitorum communis, EMU: extensor metacarpi ulnans, EMR: extensor metacarpi radialis, EIL: extensor incidus longus, FCU: flexor carpi ulnaris. n= 2 embryos for *dnCXCR7* and one embryo for *CXCR7*. P values were analysed by non-parametric Mann-Whitney test using the Graphpad Prism V6 software. Error bars indicate the standard deviation. Bar: 2 mm

Figure 3: Overexpression of a dominant negative form of CXCR7 inhibits myoblast fusion *in vivo*. Immunostaining for MF20 (a, c, f) and in situ hybridization for *CXCR7* (b) on transverse sections of E10 *dnCXCR7*-infected (b, c, f) and control (a, f) limbs, showing that infected dorsal limb muscles exhibited decreased surfaces when compared to control muscles (d, f). Dorsal at the top, posterior at the left, u: ulna, r: radius. f illustrates transverse sections taken from the same longitudinal level in control and infected EMU muscle (section levels of the limb are schematized in e). *DnCXCR7*-infected muscles differentiated normally, as shown by the unchanged number of MYOG+ cells (g), but exhibited a decrease in the number of MYOG+ nuclei into the myotubes (h, i, arrows: MYOG+ nuclei in myotubes, arrowheads: MYOG+ nuclei outside myotubes) and in myoblast fusion index (j, k) when compared to controls. Arrow in k highlighted the few myotubes in control exhibiting two neighbour nuclei, which are never observed in *Dn-CXCR7* expressing muscles. n= 7 embryos. ANC: anconeus, EDC: extensor digitorum communis, EML: extensor medius longus, EMU: extensor metacarpi ulnans, EIL: extensor incidis longus. P values were analysed by non-parametric Mann-Whitney test using the Graphpad Prism V6 software. Error bars indicate the standard deviation. Bars: 200 µm in a-c; 100 µm in d; 50 µm in f, 25 µm in i, k.

Figure 4: CXCR7 overexpression promotes myoblast fusion *in vivo.* Immunostaining for MF20 (a, c, f) and in situ hybridization for *CXCR7* (b) on transverse sections of *CXCR7*-infected (b, c, f) and control (a, f) limbs, showing that infected dorsal limb muscles exhibited increased surfaces when compared to control muscles (d, f). Dorsal at the top, posterior at the

left, u: ulna, r: radius. f illustrates transverse sections taken from the same longitudinal level in control and infected EDC muscle (section levels of the limb are schematized in e). *CXCR7*-infected muscles differentiated normally, as shown by the unchanged number of MYOG+ cells (g), but exhibited an increase in the number of MYOG+ nuclei into the myotubes (h, i, arrows: MYOG+ nuclei in myotubes, arrowheads: MYOG+ nuclei outside myotubes) and in myoblast fusion index (j, k) when compared to controls. Arrows in k highlighted the increase in myotubes exhibiting two neighbour nuclei in *CXCR7* expressing muscles, when compared to controls. n=6 embryos. ANC: anconeus, EDC: extensor digitorum communis, EIL: extensor incidis longus, EMU: extensor metacarpi ulnans. P values were analysed by non-parametric Mann-Whitney test using the Graphpad Prism V6 software. Error bars indicate the standard deviation. Bars: 200 µm in a-c; 100 µm in d; 50 µm in f, 25 µm in i, k.

Figure 5: CXCR7 receptor controls myoblast fusion *in vitro*. (A) *dnCXCR7* overexpression in cultured foetal myoblasts decreases the number of myotubes compared to controls, as shown by MF20 immunostaining (Aa, b) and myotube quantification (Ac), without changing the total number of MYOG+ cells (Ad-f). A decrease in the number of MYOG+ myonuclei into myotubes (Ad, e, g), in myoblast fusion index (Ah) and in the number of nuclei per myotube (Ai) shows that *dnCXCR7* overexpression induced a decrease in myoblast fusion *in vitro*. *TMEM8C* expression is not affected by *dnCXCR7* overexpression (Aj). Quantification and mRNA levels of controls were normalized to 1. n=24 cultures, 8 independent experiments. (B) *CXCR7* overexpression increases the number of myotubes compared to control cultures, as shown by MF20 immunostaining (Ba,b) and myotube quantification (Bc), without modifying the total number of MYOG+ cells (Bd-f). An increase in the number of MYOG+ myonuclei into myotubes (Bd, e, g), in myoblast fusion index (Bh) and in the number of nuclei per myotube (Bi) illustrates that *CXCR7* overexpression led to an increase in myoblast fusion *in vitro*. *TMEM8C* expression is not affected by *CXCR7* overexpression (Bj). Quantification and mRNA levels of controls were normalized to 1. n=18 cultures, 6 independent experiments. P values were analysed by non-parametric Mann-Whitney test using the Graphpad Prism V6 software. Error bars indicate the standard deviation. Bars: 100 µm

Figure 6: TMEM8C and CXCR7 regulate independently myoblast fusion events during foetal myogenesis. (A) In situ hybridization of *TMEMC8* and *CXCR7* on transverse sections of chick forelimbs at E5 (a-c, dorsal at the top), E6 (d-f, dorsal muscle mass) and E10 (g-I,

FCU muscle) with simultaneous detection of DAPI in d,e and MF20 in g, h. c, f, i: Artificial superposition of *TMEMC8* and *CXCR7* expression from two adjacent sections. c, f: Higher magnification of the region squared in a,b and d,e. Arrows in g, i delineates *CXCR7* expression at the MTJ in E10 FCU muscle while arrowhead in h, i shows *TMEM8C* expression in the central region of the muscle. (B) *TMEM8C* expression is not affected by deregulation of *CXCR7* signaling. (a) RT-qPCR for *CXCR7* and *TMEM8C* on control and *dnCXCR7*-transfected (a) or *CXCR7*-transfected (b) limbs. Quantification and mRNA levels of controls were normalized to 1. P values were analysed by non-parametric Mann-Whitney test using the Graphpad Prism V6 software. (b) In situ hybridization for *TMEM8C* and *CXCR7* on transverse limb sections of *CXCR7*-infected and contralateral E8 limbs. n=6 embryos, 3 independent experiments. (C) Fusion effect of *CXCR7* occurs independently of *TMEM8C*. Expression of *SiRNA* against *TMEM8C* in cultured foetal myoblasts decreases myoblast fusion when compared to controls, as shown by MF20 immunostaining (Ca) and fusion index quantification (Cb), while coexpression of *SiTMEM8C* and *CXCR7* restores myoblast fusion at a higher level than *SiTMEM8C* but at a lower level than *CXCR7* (Ca, b). n=4 cultures. Bars: 100 µm in Aa, b, d-f; 50µm in Ag-i; 200µm in Bc.

Figure 7: CXCR7 modulates myoblast fusion through EGF receptor signaling. (A) Immunostaining for MF20 and pEGFR on transverse sections of E6 chicken limbs (Aa, dorsal muscle mass) and immunostaining for MF20, pEGFR, DAPI and CXCR7 on transverse sections of E8 limbs (Ab-e) showing the expression of pEGFR in muscle nuclei from E8 of development. c, d represent high magnification of the squared region in b. ANC: anconeus, EIL: extensor incidis longus, EMU: extensor metacarpi ulnans. (B) Immunostaining for PAX7 (Ba), MF20 (Bb) and pEGFR (Ba, b) on chicken foetal myoblasts cultured for 3 days showing the diffuse expression of pEGFR in the cytoplasm of PAX7+ myoblasts and the nuclear pEGFR expression in differentiated myotubes. (C) Inhibition of pEGFR blocks the CXCR7-dependent myoblast fusion. Control (Ca-c), PD153035-treated (Cd-f), *CXCR7*-transfected cultures (Cg-i) and *CXCR7*-transfected cultures treated with PD153035 (Cj-l) and stained with MF20 and pEGFR. (m) Quantification of myoblast fusion index in control, PD153035-treated, *CXCR7*-transfected cultures and *CXCR7*-transfected cultures treated with PD153035. Myoblast fusion was blocked by inhibition of EGFR phosphorylation and CXCR7 gain-of-function was not able to restore the myoblast fusion defect demonstrating that CXCR7 effect on myoblast fusion acts through EGFR phosphorylation. n=24 cultures, 4 independent experiments. Bars: 100µm. b, c, e, f and h, i, k, l represent high magnifications of

the squared regions in a, d and g, j respectively. P values were analysed by non-parametric Mann-Whitney test using the Graphpad Prism V6 software. Error bars indicate the standard deviation.

Figure 8: CXCL12 overexpression in CT promotes myoblast fusion in chicken limb muscles (A) Lateral plate electroporation was performed in E2.5 embryos and electroporated limbs expressing TOMATO were collected at E9 (Ab). (B) MF20 immunostaining in electroporated (Bb, e) and control (Ba, e), showing that limb muscles exhibited increased surfaces upon CXCL12 overexpression in limb CT when compared to control muscles (c, e). f illustrates transverse sections taken from the same longitudinal level in control and EDC muscle upon CXCL12 overexpression in limb CT (section levels of the limb are schematized in d). Dorsal at the top, posterior at the left, u: ulna, r: radius. CXCL12 expression in CT did not change the total number of MYOG+ cells (Bf), but induced an increase in the number of MYOG+ nuclei into the myotubes (Bg, h, arrows: MYOG+ nuclei in myotubes, arrowheads: MYOG+ nuclei outside myotubes) and in myoblast fusion index (Bi,j) when compared to controls. Arrows in j highlighted myotubes exhibiting two neighbour nuclei in nearby muscles of *CXCL12* overexpression in CT. ANC: anconeus, EDC: extensor digitorum communis, EML: extensor medius longus, EMU: extensor metacarpi ulnans, FCU: flexor carpi ulnaris. n= 9 embryos. Bars: 200 µm in a, b; 100 µm in c; 50 µm in e, 25 µm in h, j. (C) RT-qPCR for *CXCL12* and *TMEM8C* on control and electroporated limbs with *CXCL12* showing that *TMEM8C* expression is not affected by CXCL12 overexpression in limb CT. Quantification and mRNA levels of controls were normalized to 1. n=6 embryos, 3 independent experiments.

Figure 9: CXCL12 overexpression in CT increases ß1integrin activation at the MTJ and promotes CXCR7 expression in muscle. (A) MF20 (a, d) and TASC (b, c) immunostaining on transverse sections of electroporated (c, d) and control (a, b) limbs, showing the increase in TASC expression in CXCL12 overexpressing limb regions (arrows in b, c). FCU: flexor carpi ulnaris. Dorsal at the top left, posterior at the bottom left, u:ulna, r: radius. (e) Quantification of FCU muscle surface in the electroporated limb overexpressing CXCL12 in CT, showing the expected surface increase attesting of the CXCL12 phenotype. The surface represents the average of all FCU muscle transverse sections in control and electroporated limb. (f-h) MF20 and TASC immunostaining (f, g) on transverse sections of control (f) and electroporated (g, h) limb regions expressing CXCL12 in CT (h). TASC expression is increased and enlarged at the MTJ in FCU muscle (arrows in f, g). Asterisk in f, g shows the increased TASC

expression around the cartilage of electroporated limb. CXCR7 and TASC immunostaining (i, j) on transverse sections of control (i) and electroporated (j) limb region expressing CXCL12 in CT (k), showing the increase and enlargement of CXCR7 expression in FCU muscle (arrows in i, j). Asterisks highlight ß1integrin activation at MTJ nearby CXCL12 overexpression in CT. n= 5 embryos. Bars: 200 µm in Aa-d; 100 µm in Af-k. (B) Integrin activation enhances myoblast fusion and CXCR7 expression *in vitro*. Control, PMA-treated, *dnCXCR7*-transfected cultures and *dnCXCR7*-transfected cultures treated with PMA and stained with MF20 (Ba, b, g, i), TASC (Bc, d, h, j) and CXCR7 (Be, f). Myoblast fusion, TASC and CXCR7 staining were increased after integrin activation by PMA (Bb, d, f) but integrin activation had no effect on myoblast fusion after CXCR7 loss-of-function (Bi, j). (k) Quantification of myoblast fusion index in control, PMA-treated, *dnCXCR7*-transfected cultures and *dnCXCR7*-transfected cultures treated with PMA. n=24 cultures, 4 independent experiments. Bars: 100 µm. P values were analysed by non-parametric Mann-Whitney test using the Graphpad Prism V6 software. Error bars indicate the standard deviation.

Figure 10: A proposed model for the regulation of myoblast fusion at foetal muscle fiber tips via CXCR7.

Legends to Supplemental Figures

Supplemental Figure 1: **CXCR4 receptor is expressed in vessels during limb development in chicken embryos.** CXCR4 (a, b), MEP21 (c) and MF20 (d) immunostaining on transverse sections of E6 chick embryo limbs. At E6, CXCR4 is no more expressed in muscle masses (b, d) but its expression is reminiscent of MEP21 staining, corresponding to endothelial cells of the limb vessels (b, c). b, c, d : high magnification of the squared region in a. Arrows indicate CXCR4 expression in vessels and arrowheads the lack of CXCR4 expression in muscle masses. Dorsal at the top, posterior at the left. *CXCL12* (e) and CXCR4 (f) staining on transverse sections of E10 chick embryo limbs showing the strong *CXCL12* expression in CT surrounding vessels (arrows). Bars : 100 µm.

Supplemental Figure 2: Deregulation of CXCL12/CXCR7 signaling does not modify myoblast proliferation and specification in chicken limb muscles (A) *dnCXCR7*-infected limb muscles exhibited no change in cell proliferation (Aa) and number of PAX7+ cells (Ab) when compared to controls. n= 7 embryos. (B) *CXCR7*-infected limb muscles exhibited no

change in cell proliferation (Ba) and number of PAX7+ cells (Bb) when compared to controls. n= 6 embryos. (C) CXCL12 overexpression in limb CT did not modify cell proliferation (Ca), and number of PAX7+ cells (Cb) in nearby muscles when compared to controls. n= 9 embryos. P values were analysed by non-parametric Mann-Whitney test using the Graphpad Prism V6 software. Error bars indicate the standard deviation.

Supplemental Figure 3: Deregulation of CXCR7 receptor does not modify myoblast proliferation and specification in chicken foetal myoblast cultures. (A) Expression of CXCR7 receptor in foetal muscle cells *in vitro*. In situ hybridization for *CXCR7* (a) and immunostaining for PAX7 (b, c), MF20 (b, d) and CXCR7 (c, d) in foetal myoblasts cultured under differentiation conditions for 3 days. Both *CXCR7* mRNA and CXCR7 protein are expressed in a few PAX7-positive cells (arrows in a, c) and around some nuclei in MF20-positive myotubes (arrowheads in a, b, d). Bars: 100 µm in a, b, d, e, f; 50µm in c. (B) *dnCXCR7* expression did not induce changes in total and PAX7+ cell proliferation (Ba) and in total number of PAX7+ cells (Bb). n=24 cultures, 8 independent experiments. (C) *CXCR7* overexpression did not induce changes in total and PAX7+ cell proliferation (Ca) and in total number of PAX7+ (Cb). n=18 cultures, 6 independent experiments. P values were analysed by non-parametric Mann-Whitney test using the Graphpad Prism V6 software. Error bars indicate the standard deviation.

Supplemental Figure 4: CXCR7 deregulation does not impair *in vitro* migration of foetal myoblasts (Aa) Measurement of gap closure in wound healing assays 48 hours after the scratch in primary cultures of chicken foetal myoblasts. (Ab) Measurement of gap closure of PAX7-positive cells in wound healing assays 48 hours after the scratch in primary cultures of chicken foetal myoblasts. (B) Phase-constrat views of gap closure in control (a), *dnCXCR7*-transfected (c) and *CXCR7*-transfected (e) cultures. Black lines delineate the gap borders. Phase-contrast views of and PAX7 immunostaining in control (b), *dnCXCR7*-transfected (d) and *CXCR7*-transfected (f) cultures. P values were analysed by non-parametric Mann-Whitney test using the Graphpad Prism V6 software. Error bars indicate the standard deviation. n=12 cultures, 3 independent experiments. Bars: 1mm in a, c, e, 100µm in b, d, f.

Supplemental Figure 5: CXCL12 does not impair *in vitro* foetal myogenesis. (A) Chicken embryonic fibroblasts were transfected with RCAS-*CXCL12* or control empty RCAS and transfected CEF were grown for 2 days to generate CXCL12 or control concentrated medium.

Mediums were used to culture myoblasts under proliferation or differentiation conditions before staining. (B) Immunostaining for MF20 (Ba, b), quantification of myotubes (Bc, d), cell proliferation (Be, f), PAX7+ cells (Bg), number of nuclei per myotube (Bh) and fusion index (Bi) all showed that CXCL12 has no effect on *in vitro* myogenesis. P values were analysed by non-parametric Mann-Whitney test using the Graphpad Prism V6 software. Error bars indicate the standard deviation. n=36 cultures, 12 independent experiments. Bar: 100 µm

Supplemental Figure 6: Integrin activation enhances CXCR7 expression and myoblast fusion in vitro. Chicken foetal myoblasts were cultured for 2 days in proliferation and Mn2+ was added to proliferating myoblasts for 3 hours. Control, Mn2+-treated, *dnCXCR7*-transfected cultures and *dnCXCR7*-transfected cultures treated with Mn2+ and stained with MF20 (a, c, e, f) and CXCR7 (b, d). Myoblast fusion and CXCR7 staining were increased after integrin activation by Mn2+ but integrin activation had no effect on myoblast fusion after CXCR7 loss-of-function. (g) Quantification of myoblast fusion index in control, Mn2+-treated, *dnCXCR7*-transfected cultures and *dnCXCR7*-transfected cultures treated with Mn2+. P values were analysed by non-parametric Mann-Whitney test using the Graphpad Prism V6 software. Error bars indicate the standard deviation. n=12 cultures, 3 independent experiments. Bars: 100 µm.

Supplemental Figure 7: CXCL12 does not impair ß1 integrin activation and *CXCR7* expression in *in vitro* foetal myogenesis. Chicken foetal myoblasts were grown with control or CXCL12 concentrated medium for 2 days under proliferation conditions and 5 days under differentiation conditions. (A) Immunostaining for MF20 (Aa, c) and TASC (Ab, d), showing that CXCL12 has no effect on ß1 integrin activation in foetal myoblast cultures. (B) RT-qPCR for *CXCR7* on foetal myoblasts cultured in control conditions or with CXCL12 concentrated medium showing that CXCL12 has no effect on *CXCR7* expression. Quantification and mRNA levels of controls were normalized to 1. P values were analysed by non-parametric Mann-Whitney test using the Graphpad Prism V6 software. Error bars indicate the standard deviation. n=18 cultures, 3 independent experiments. Bar: 100 µm

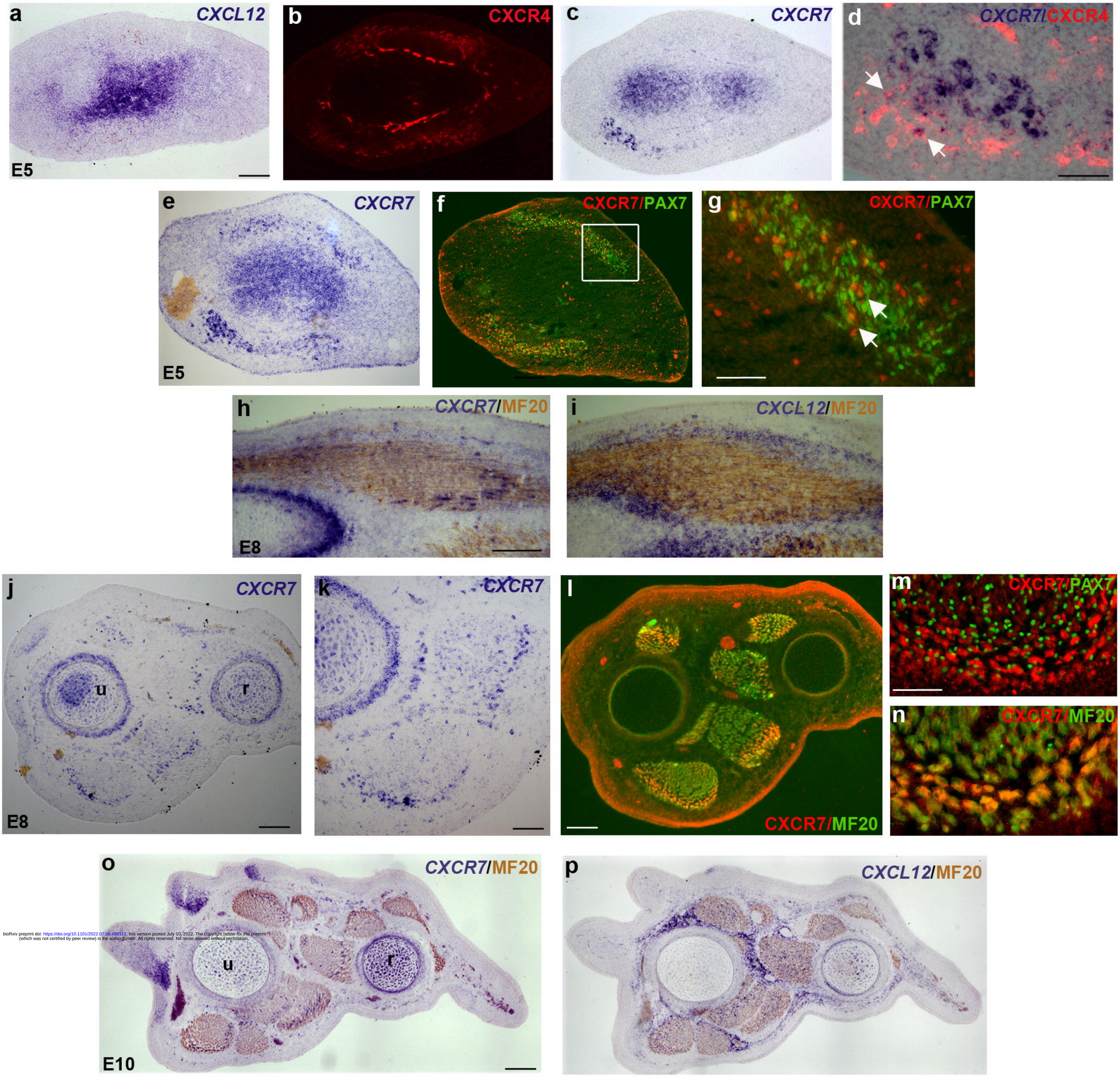

Figure 1

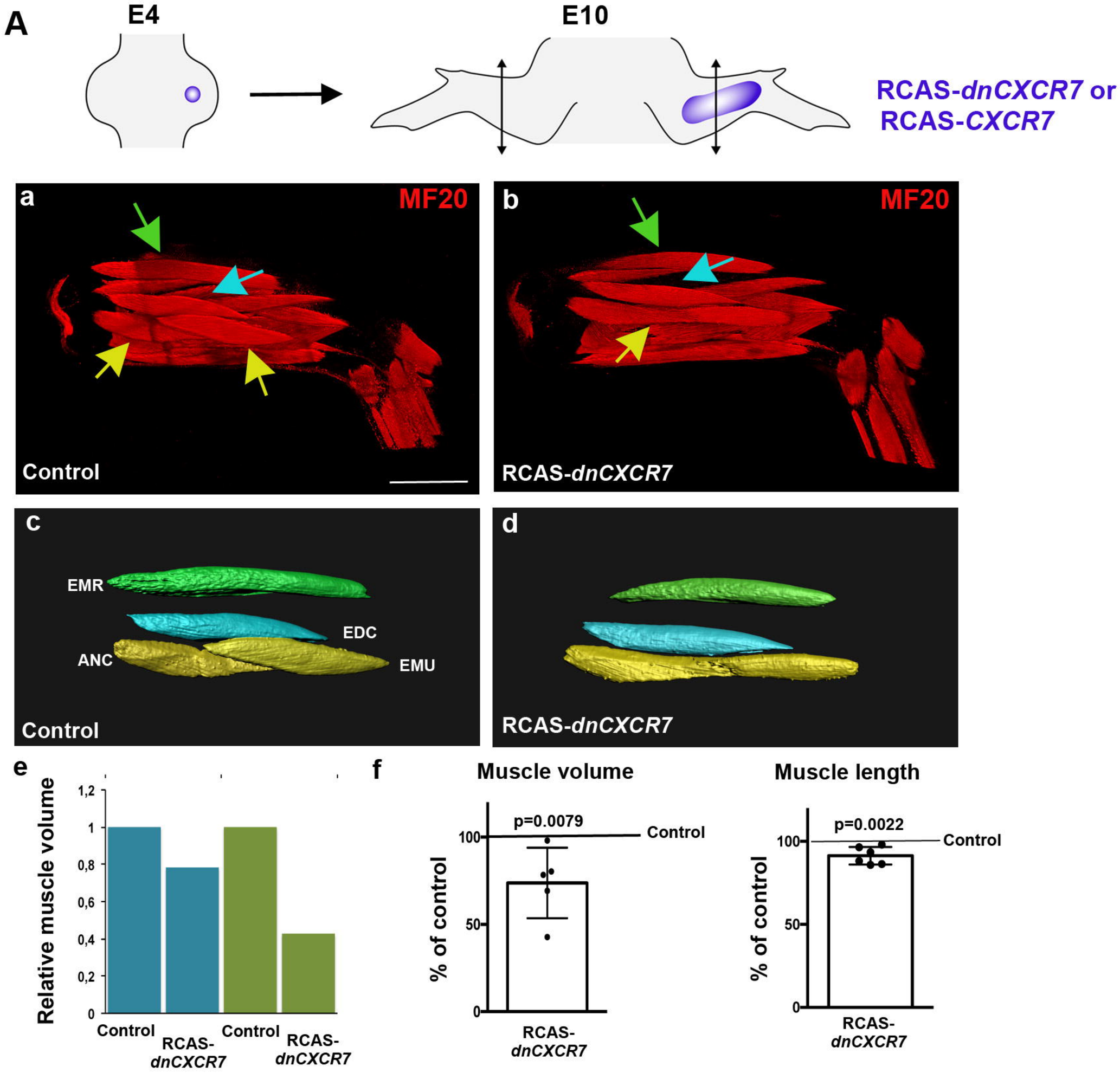

Figure 2

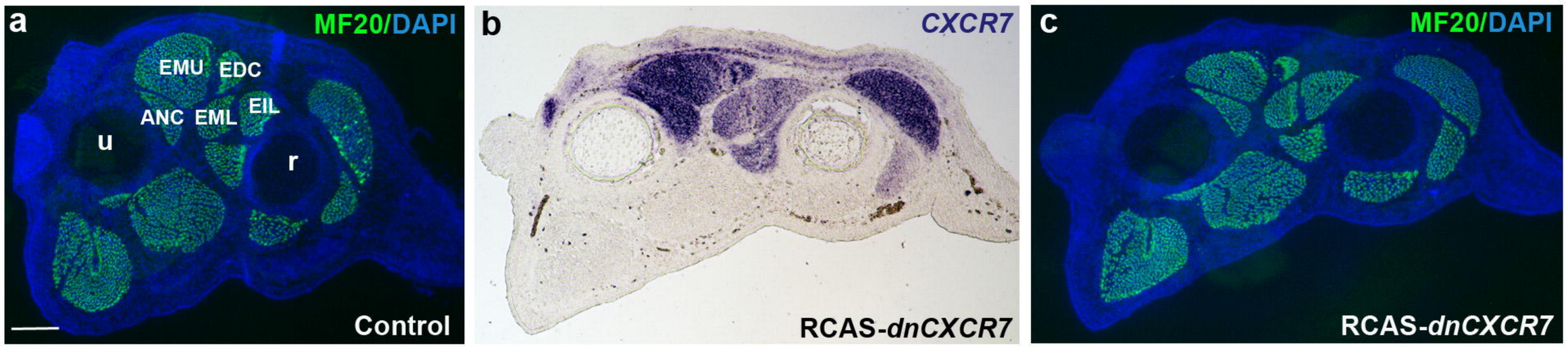

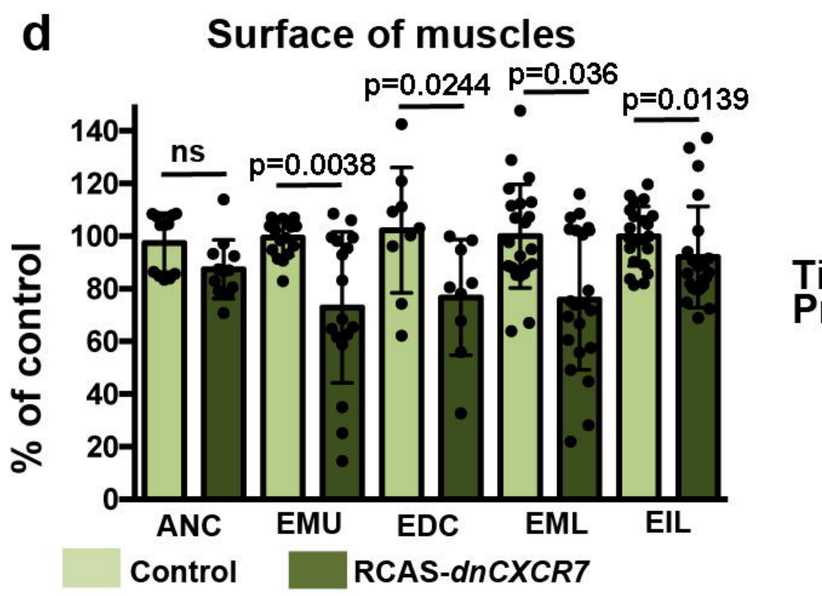

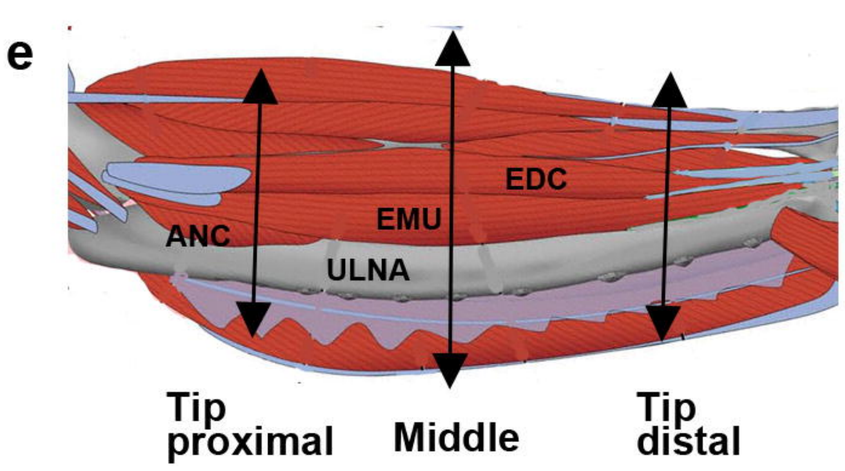

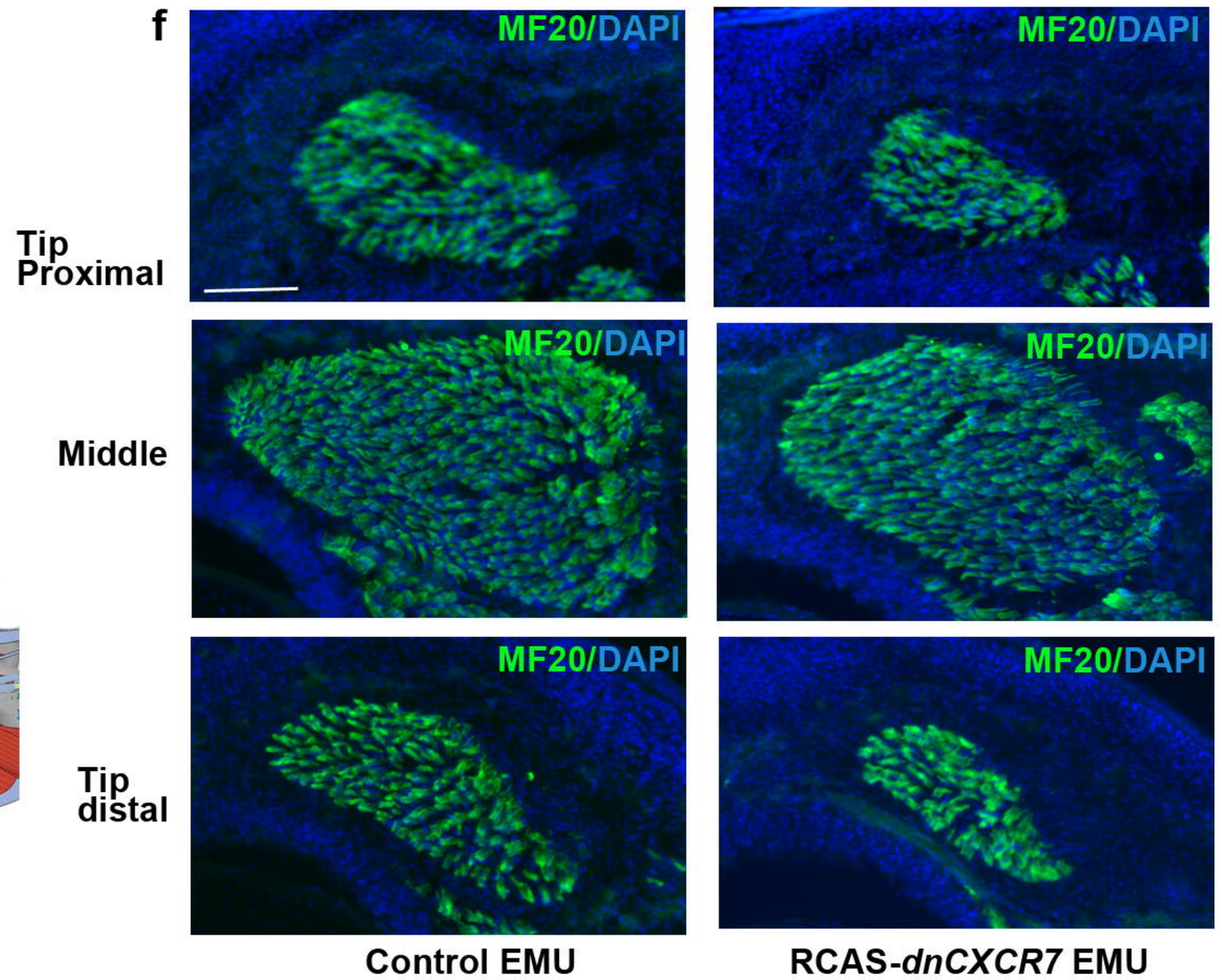

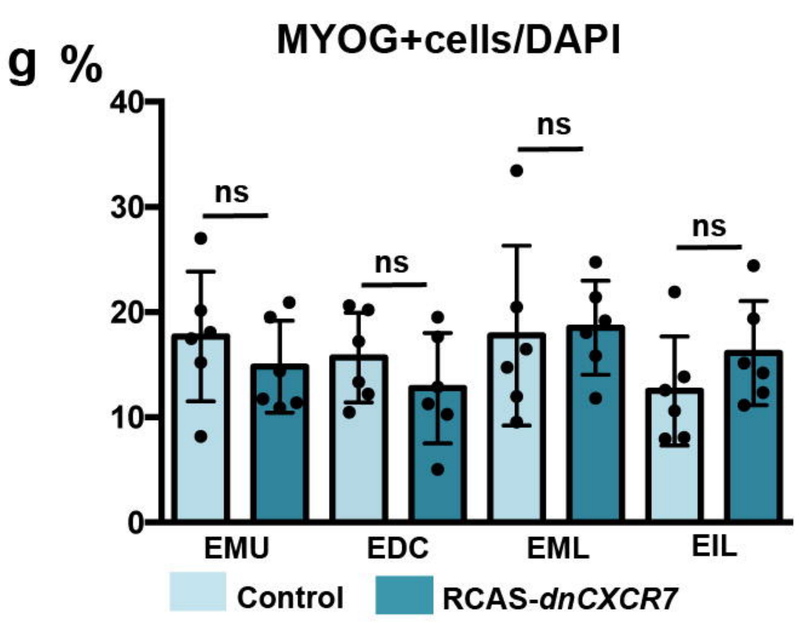

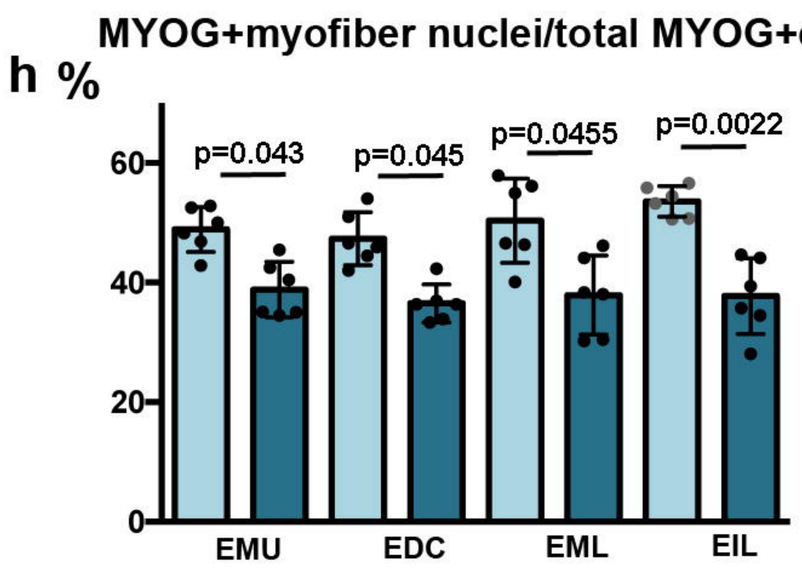

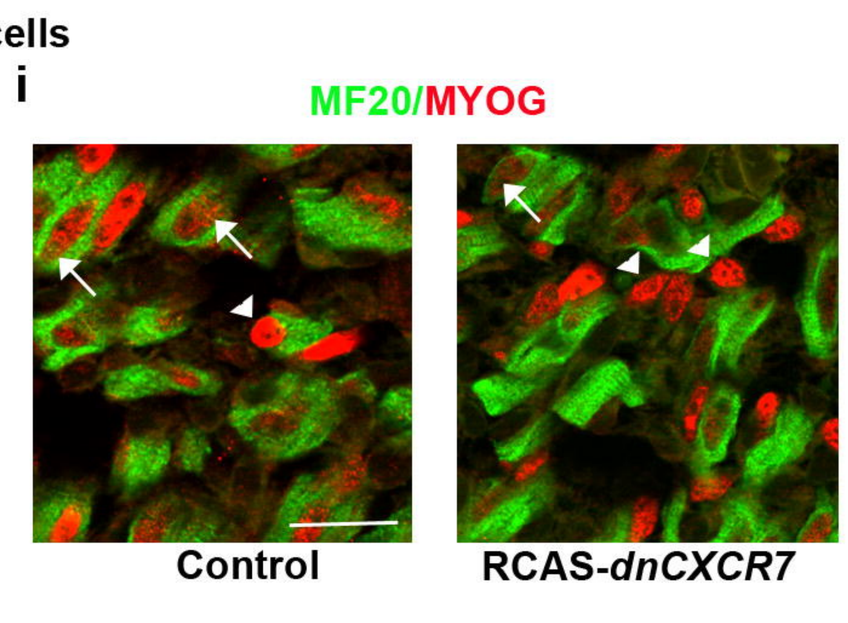

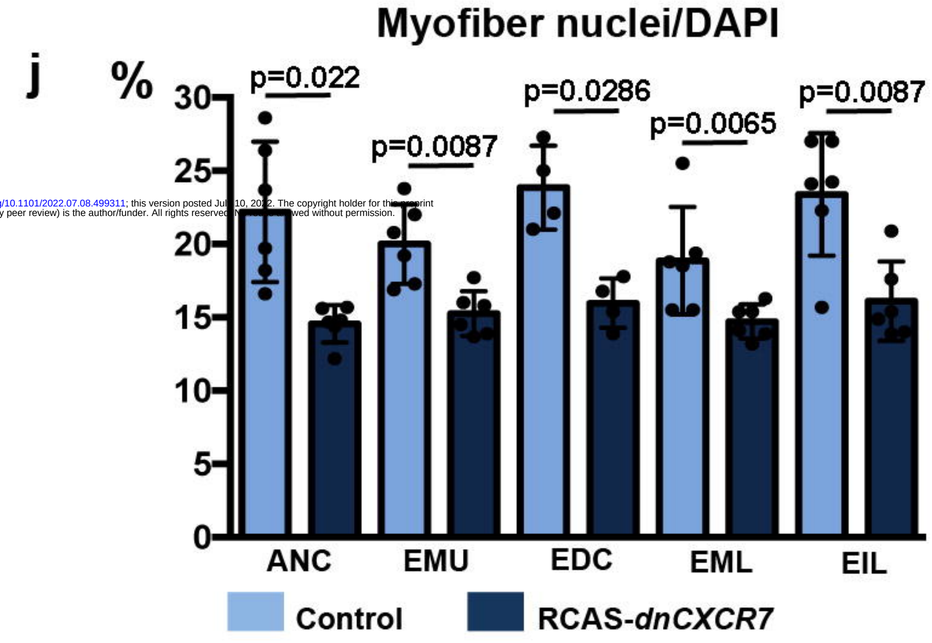

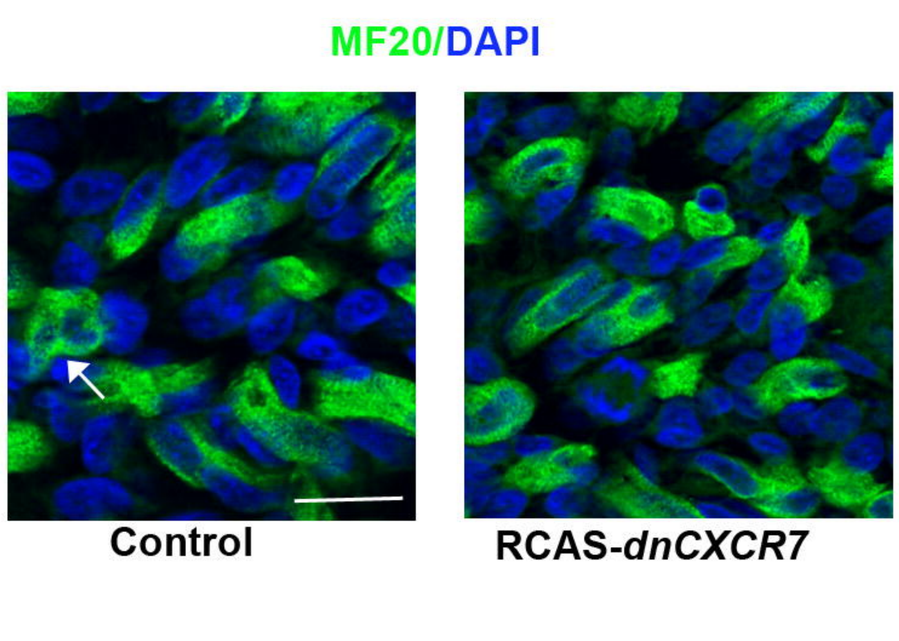

Figure 3

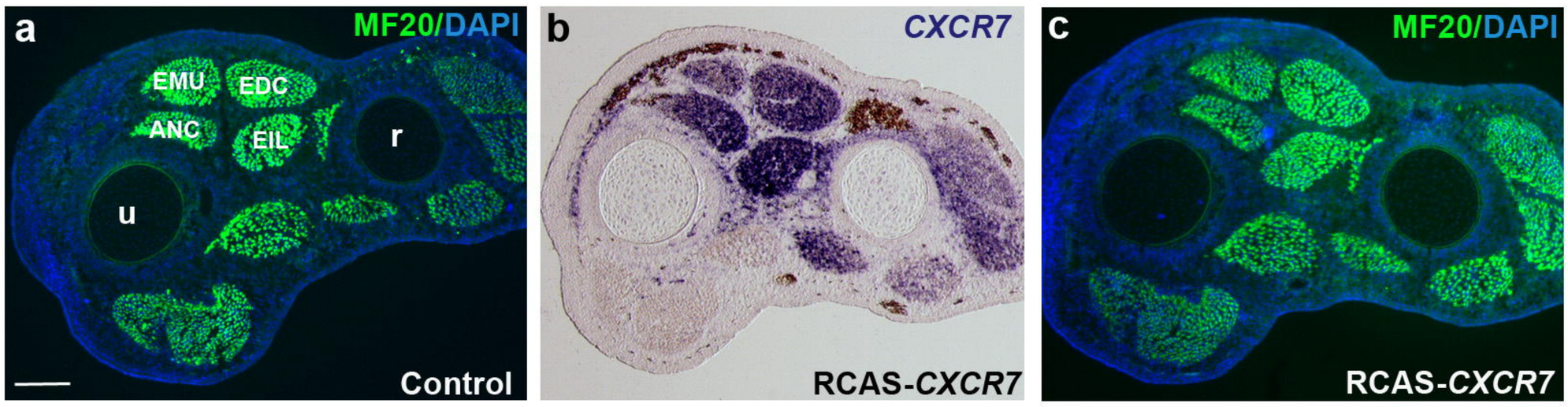

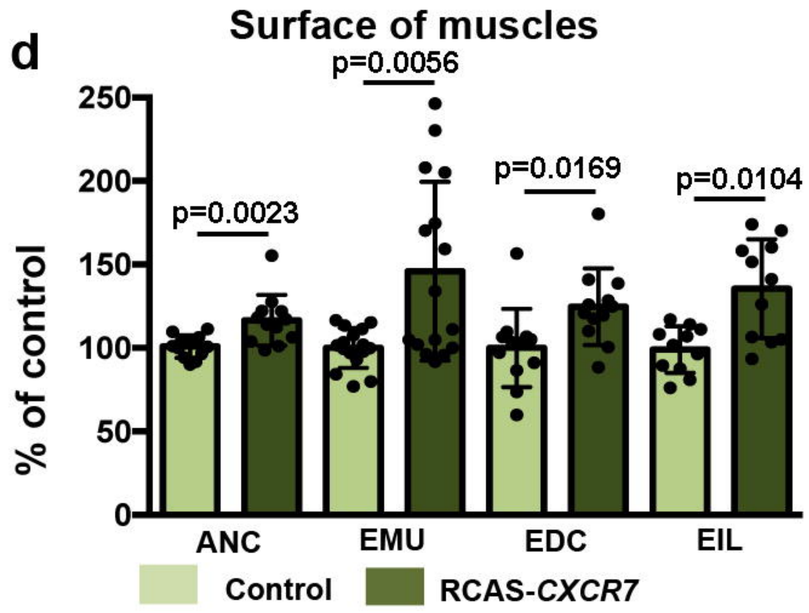

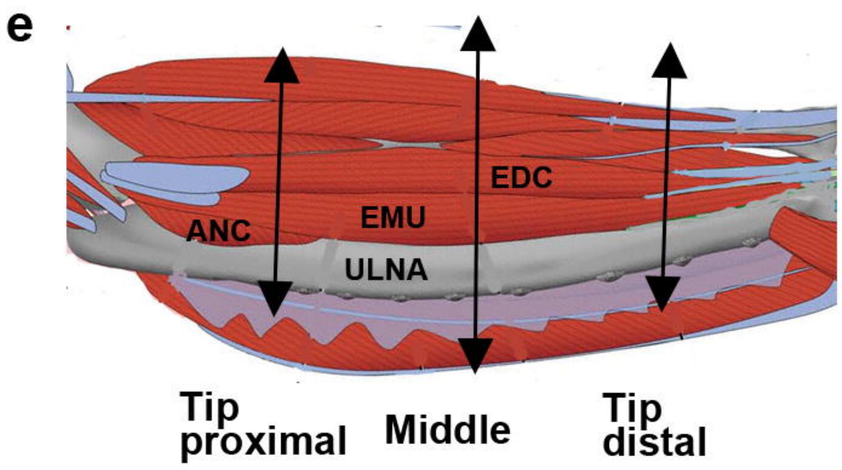

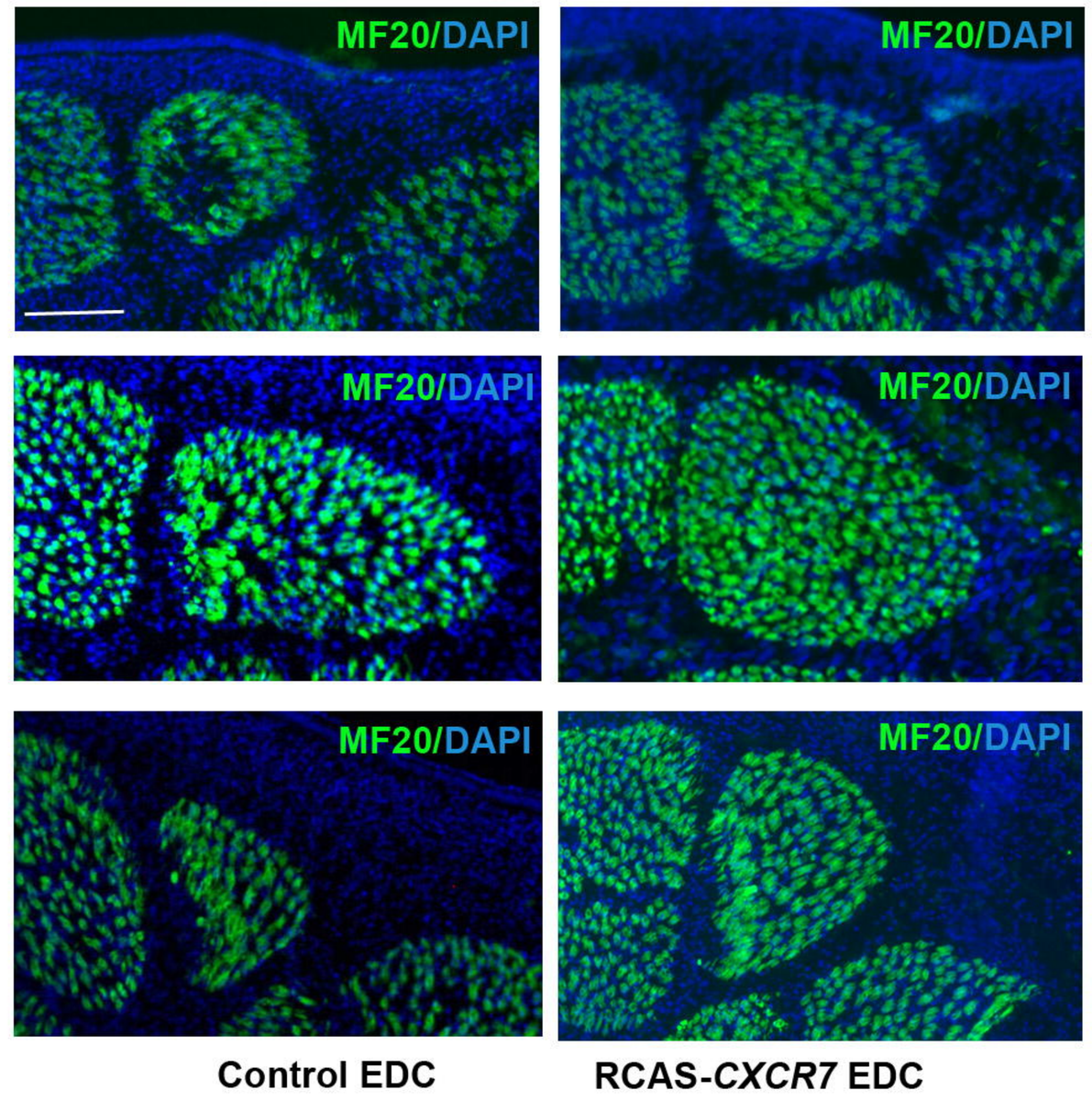

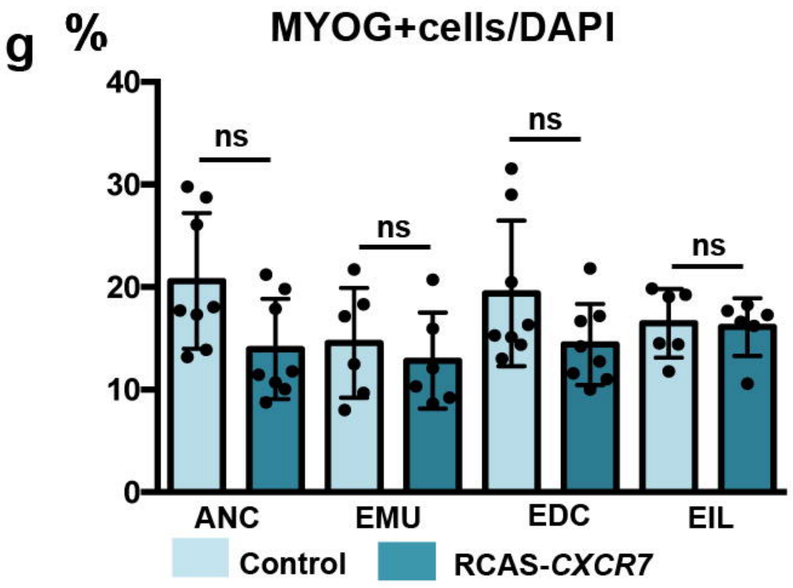

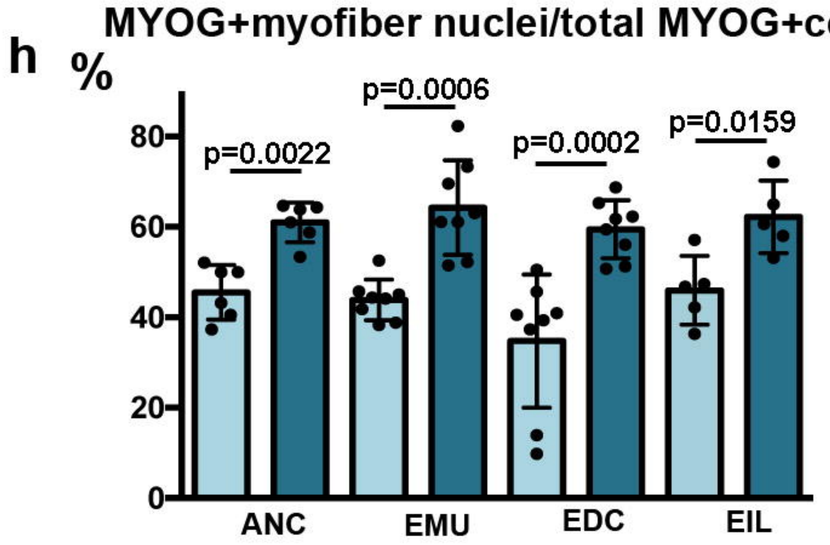

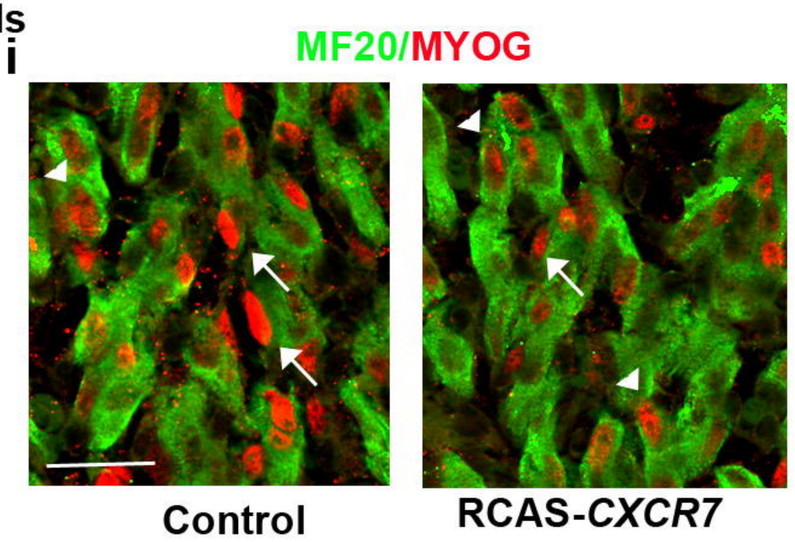

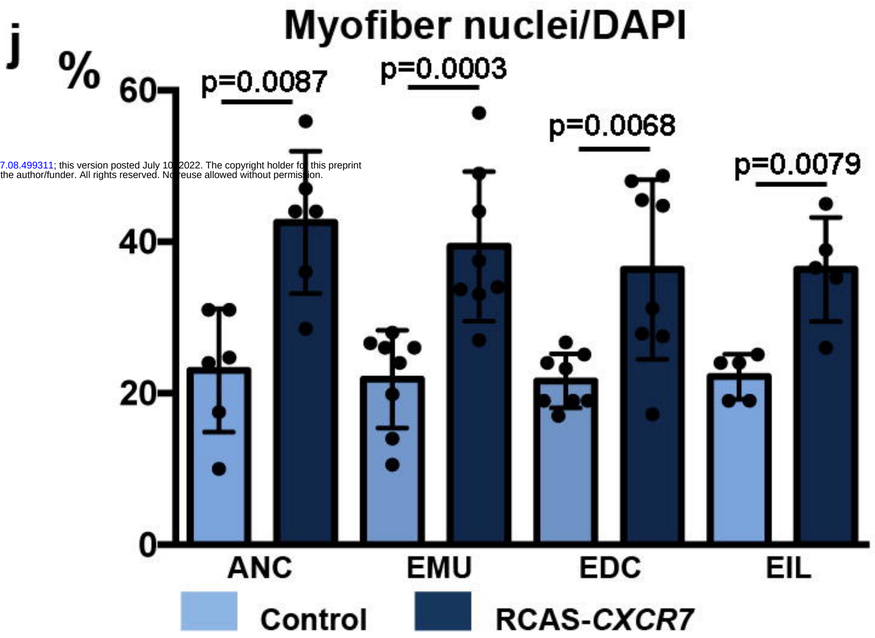

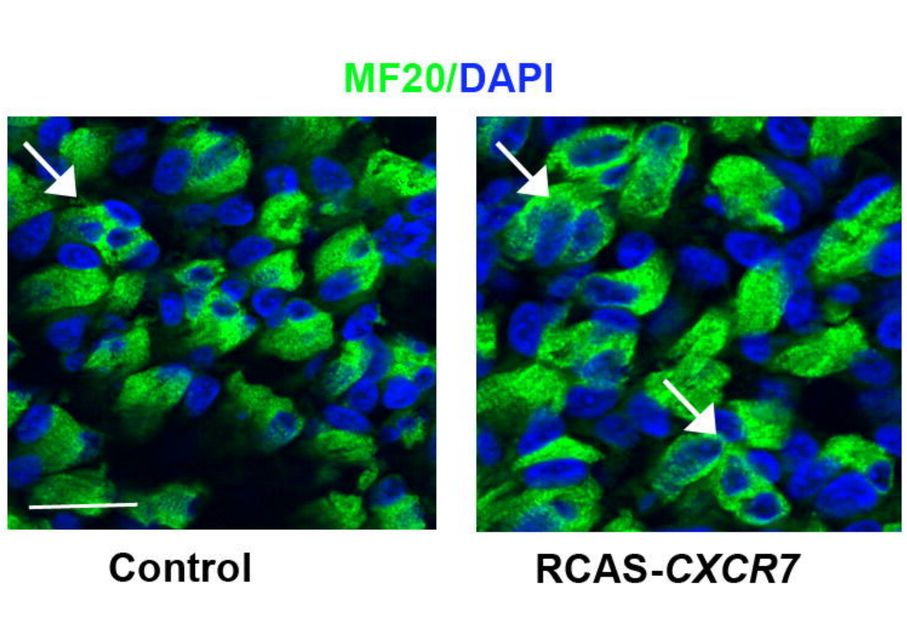

Figure 4

A

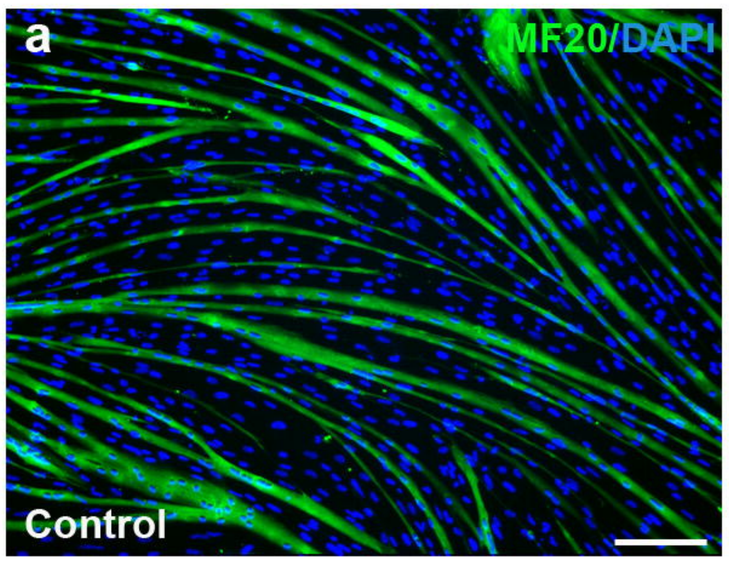

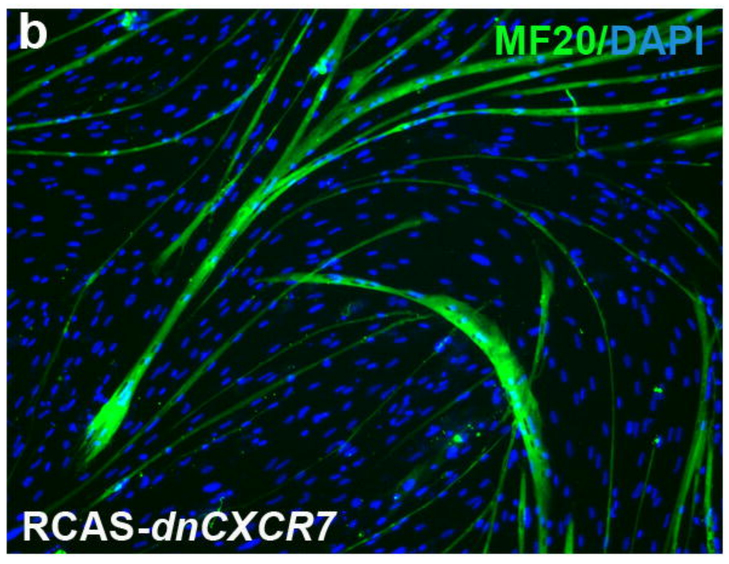

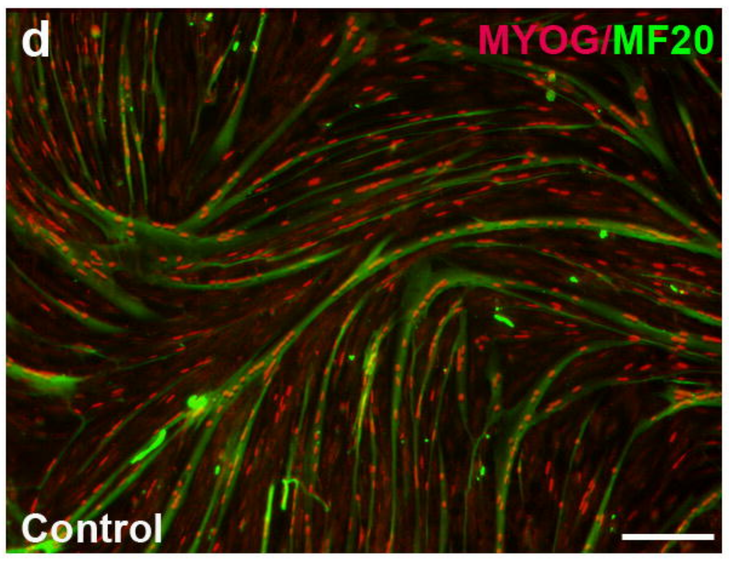

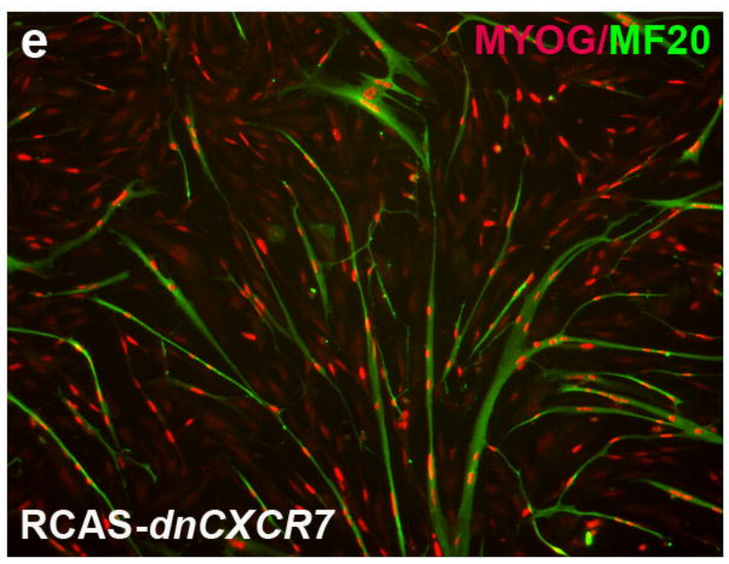

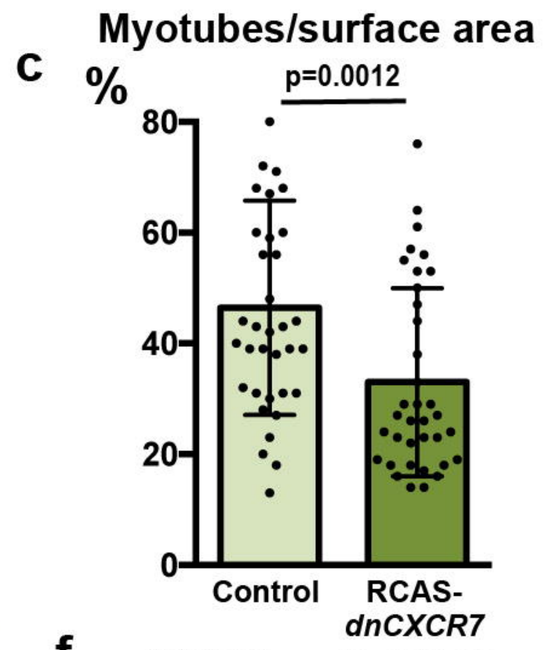

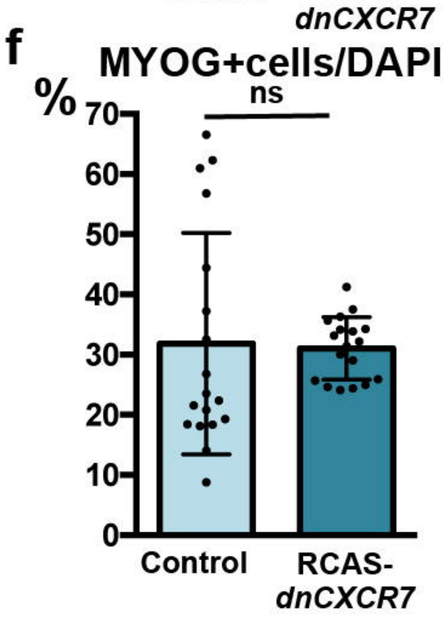

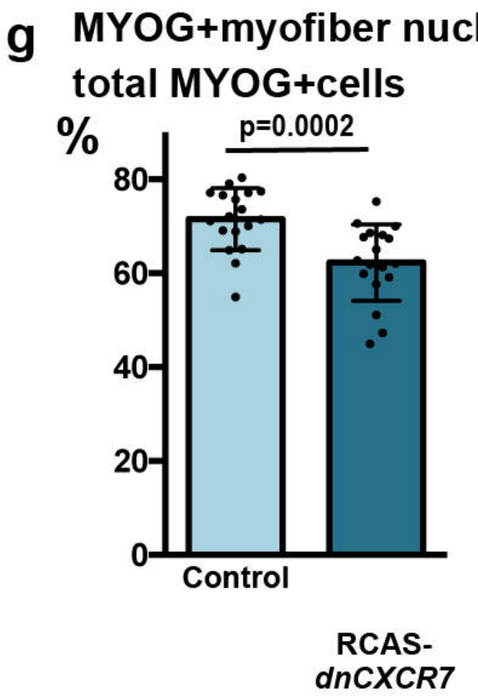

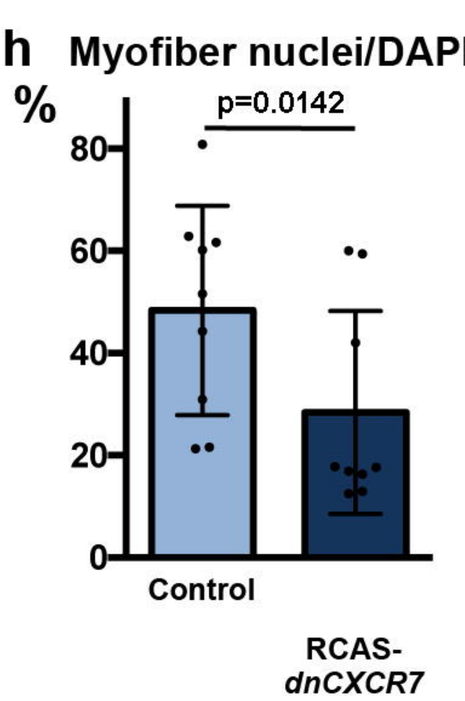

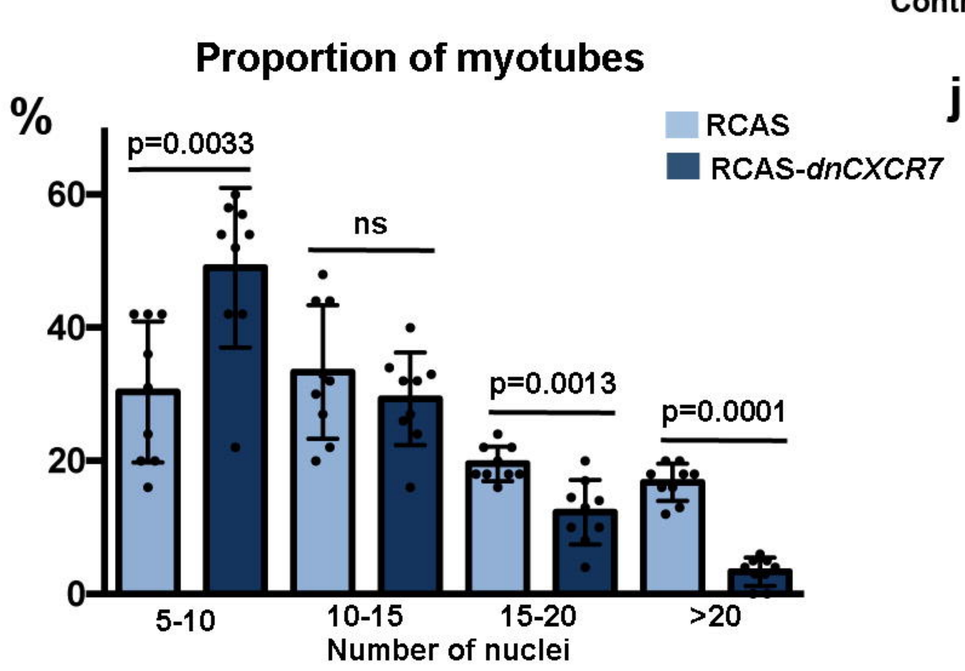

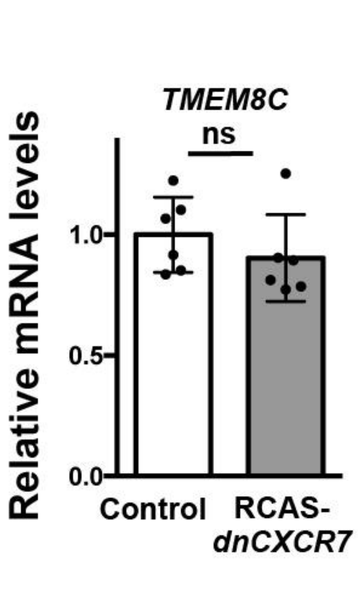

B

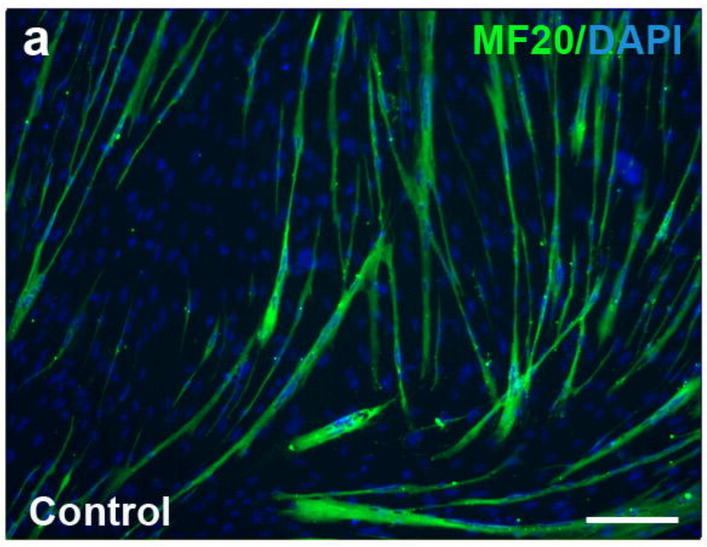

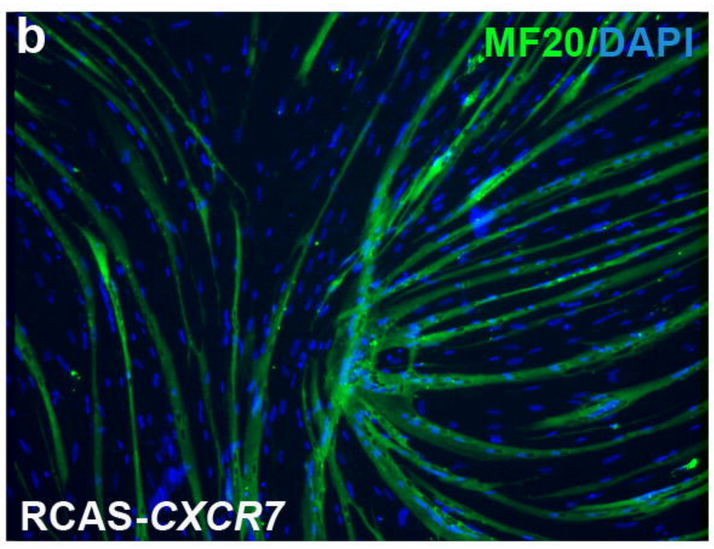

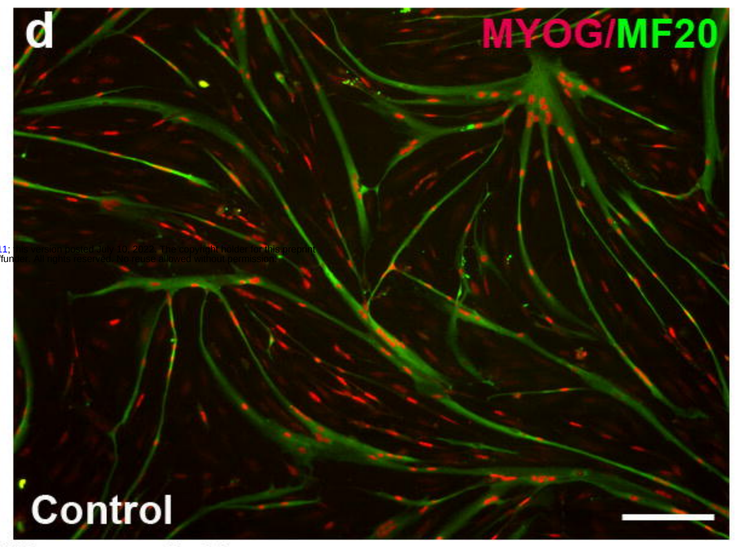

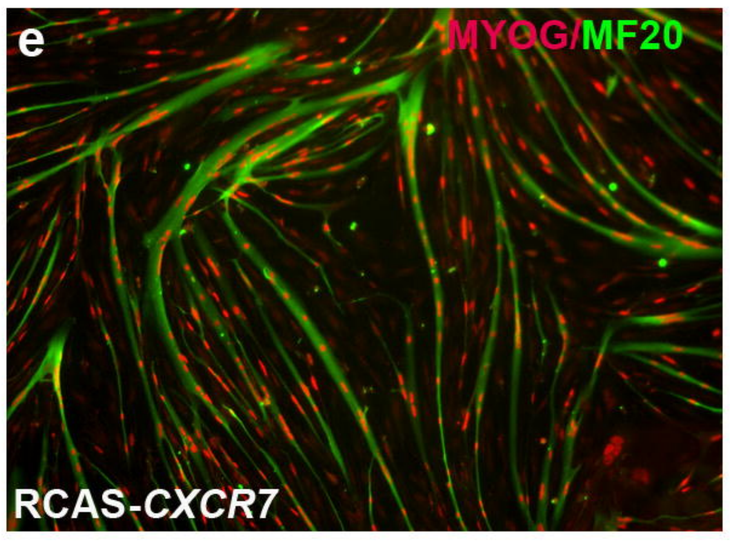

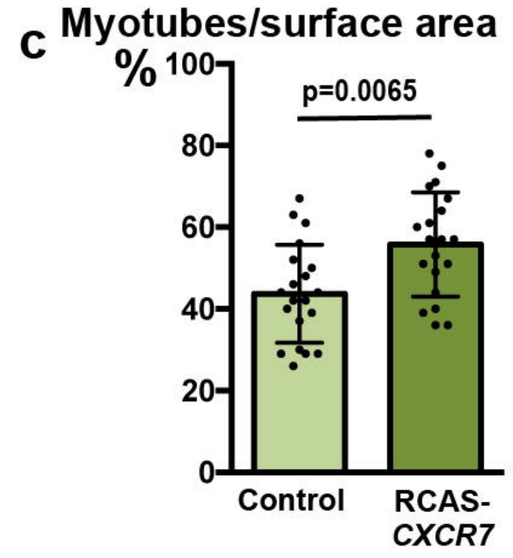

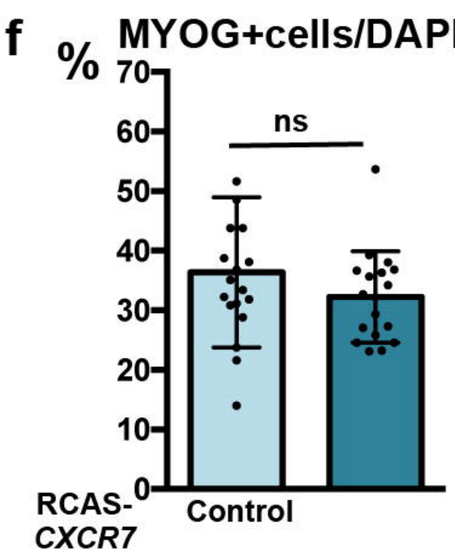

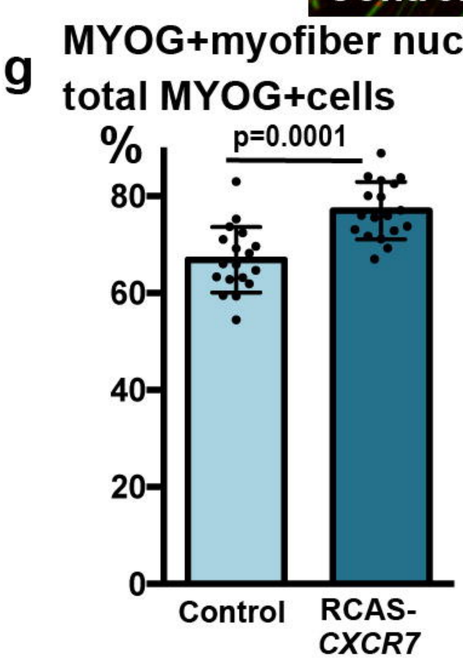

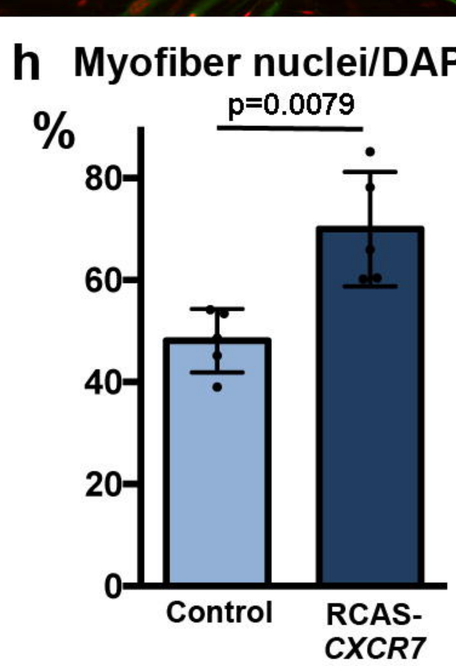

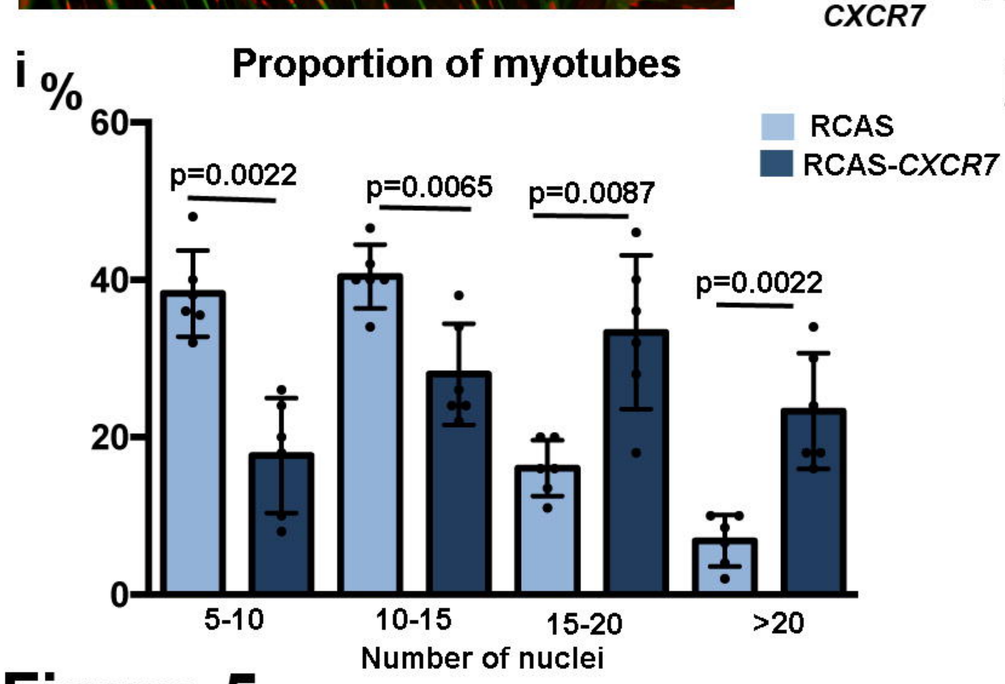

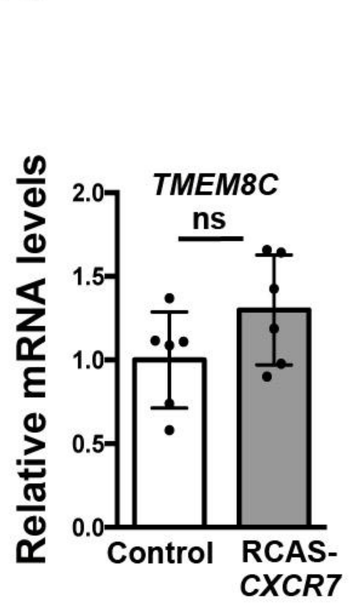

Figure 5

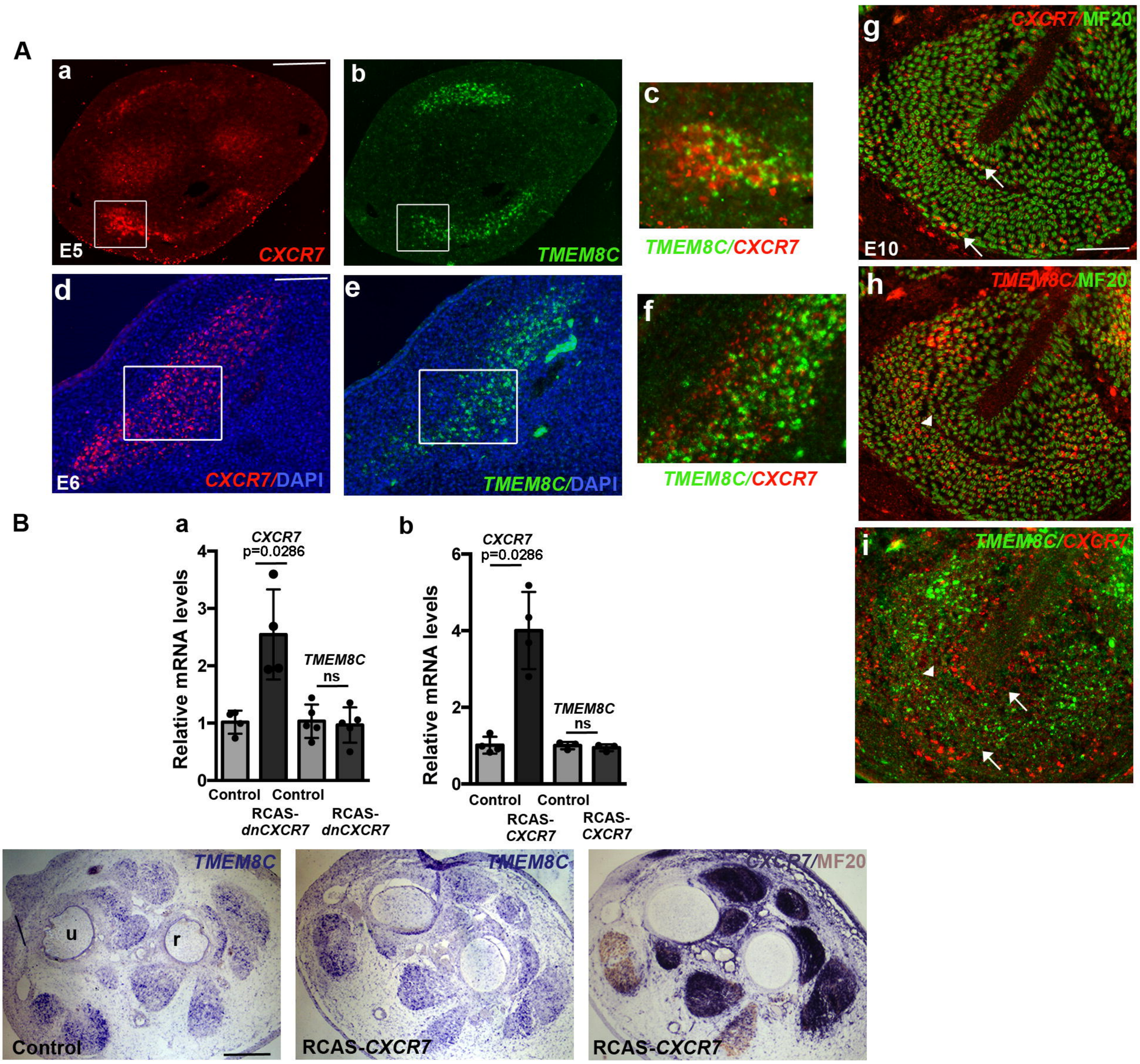

Figure 6

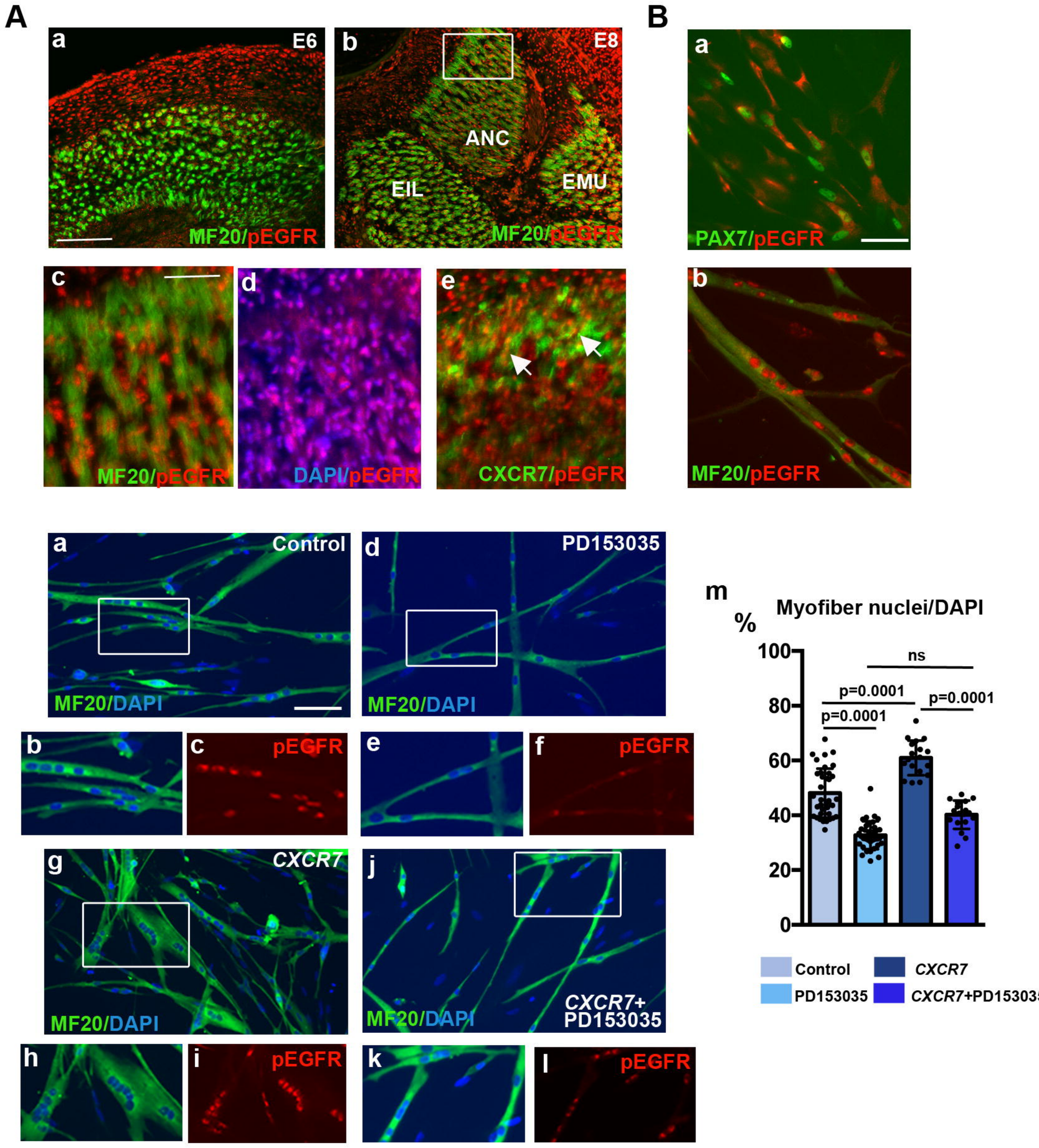

Figure 7

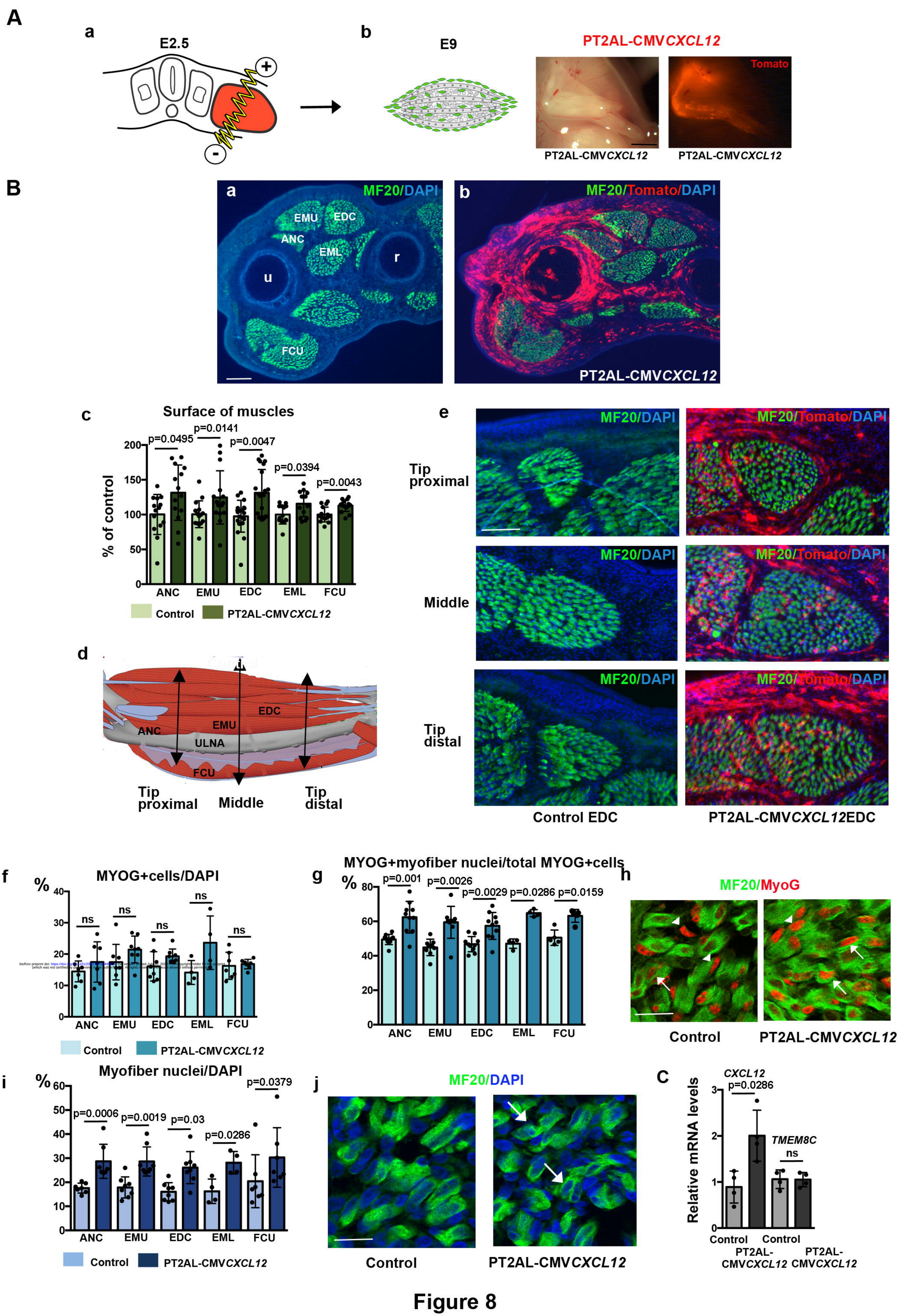

Figure 8

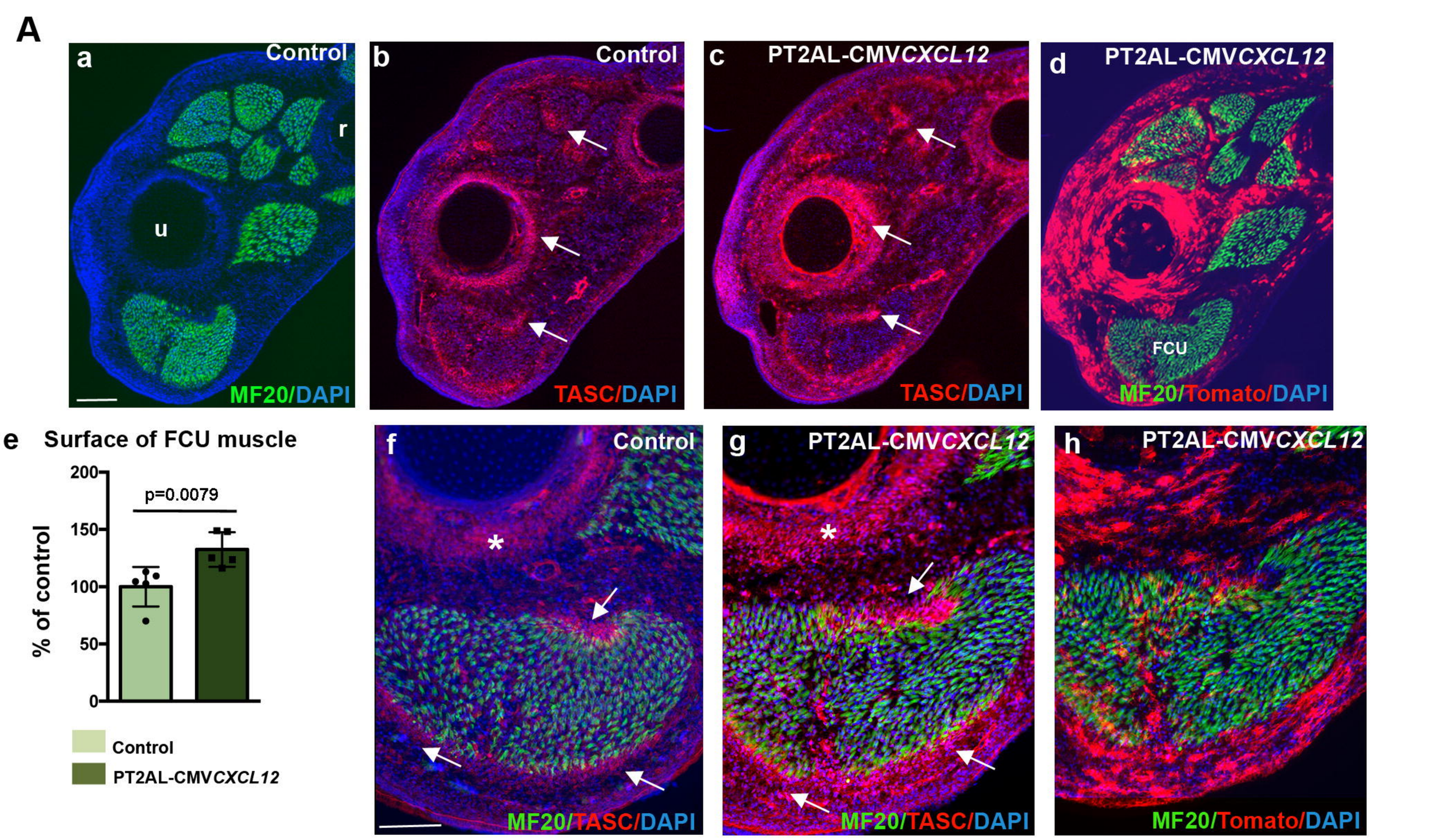

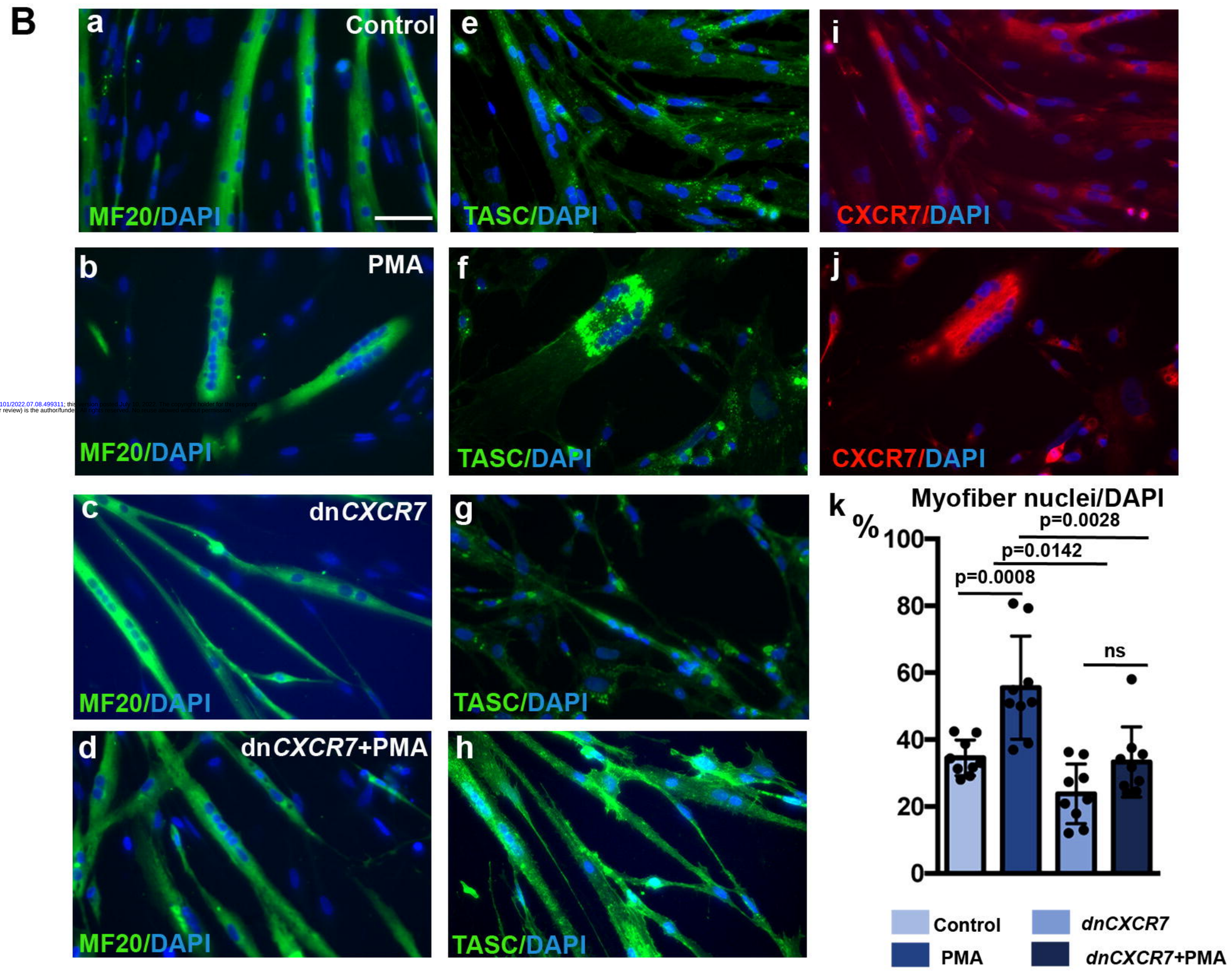

Figure 9

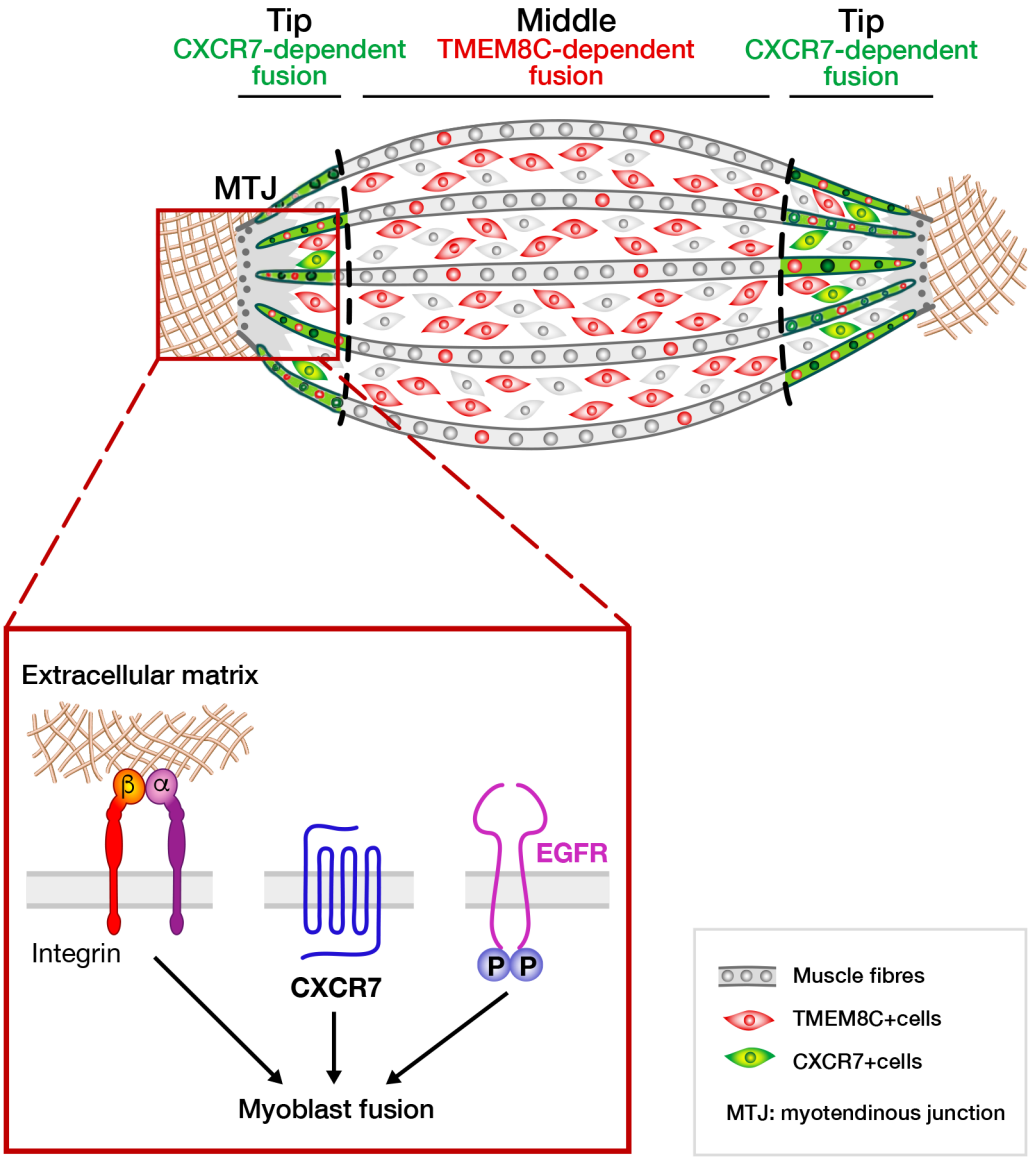

Figure 10